Multiphoton processes in an intense laser field: Harmonic generation and total ionization rates for atomic hydrogen

R. M. Potvliege and Robin Shakeshaft
Department of Physics, University of Southern California, Los Angeles, California 90089-0484
(Received 16 January 1989)

We report results of large-scale nonperturbative (Floquet) calculations of rates for harmonic generation and total ionization of H(1*s*) by fields whose intensity ranges from about 10^{12} to 3×10^{13} W/cm^2 and whose wavelength ranges from 265 to 1064 nm. At long wavelengths and moderate to high intensities, perturbation theory yields estimates of total ionization rates that are orders of magnitude too large, and estimates of harmonic-generation rates that exhibit a qualitatively incorrect behavior with respect to order. We have studied the influence of resonances on the ionization rates, and we illustrate the resonance enhancement of the ionization yield for a realistic pulse. Finally, we address several formal aspects of Floquet theory, including the convergence of the induced dipole moment, gauge invariance, and the normalization of the wave function.

I. INTRODUCTION

In this paper we report results of a nonperturbative calculation of rates for high-order harmonic generation and total ionization for atomic hydrogen in a strong oscillating field. We consider the field to have an intensity in about the range $10^{12}-3\times10^{13}$ W/cm^2 and a wavelength in the range 265–1064 nm. We compare our results with those obtained using lowest-order perturbation theory, and we often find pronounced differences.

Previous results of large-scale nonperturbative calculations of ionization rates for hydrogen[1–5] are rather sparse, and are limited to relatively short wavelengths. Here we present a fairly detailed study of the quasienergy eigenvalue spectrum for hydrogen, and we depict the behavior of the eigenvalues with respect to intensity. The real and imaginary parts of these eigenvalues exhibit multiple crossings, both real and avoided, as the intensity varies. The imaginary part of an eigenvalue is proportional to the total ionization rate from the corresponding dressed state. We find that at long wavelengths and moderate to high intensities, perturbation theory yields results for total ionization rates from the ground state that are orders of magnitude too large. Thus, contrary to what perturbation theory implies, at long wavelengths an atom can experience the peak intensity of a fairly powerful laser pulse before undergoing ionization. The breakdown of perturbation theory may be predicted by considering three parameters. They are the ratio of the ponderomotive energy shift to the photon energy, the ratio of the excursion speed (of a free electron oscillating in the field) to the initial atomic orbital speed, and the ratio of the excursion amplitude to the initial atomic orbital radius; if any of these parameters is of the order of, or exceeds, unity, perturbation theory becomes inadequate. The first parameter is a measure of the increase in the minimum number of photons which the atom must absorb to ionize, and the third parameter is a measure of the degree to which the field pulls the electron away from the region near the nucleus, the region where it can absorb photons; both effects tend to reduce the ionization rate. However, the role of intermediate resonances is also important. We discuss the effect of intermediate resonances on the ionization rates, and we show that ionization is not always enhanced at resonance. We illustrate the effect of resonances on the ionization yield for a realistic pulse which has an intensity profile that is Gaussian in space and time.

There are no previous results, as far as we are aware, of nonperturbative calculations of harmonic-generation rates for hydrogen.[6] However, results obtained from lowest-order perturbation theory do exist.[7–10] We find that, in the context of harmonic generation, perturbation theory yields results which exhibit a dependence on the order of the harmonic which is qualitatively different from that of the nonperturbative results. Interest in harmonic generation in intense fields has been stimulated by the recent experimental observations of high-order harmonic generation in rare gases, both at short[11] and long[12] wavelengths. Unfortunately, we cannot compare our results directly with experimental data, not only because our results are for hydrogen, rather than the rare gases, but also because we do not take into account phase matching of the generated beam. Nevertheless, we tentatively attempt a qualitative comparison.

Our calculations are based on a time-independent (Floquet) theory, which has undergone substantial development[13–16] since its introduction;[17] in Sec. II and Appendixes A and B we continue to examine formal aspects of the theory. We assume that the field is monochromatic and spatially homogeneous. We use a complex Sturmian basis set to solve the Floquet eigenvalue equations, that is, Eqs. (1.6) below. This basis set has proved to be very useful in calculating partial differential rates for N-photon ionization, for both weak[10,18] and strong[3] fields. For weak fields, when perturbation theory is valid, Eqs. (1.6) simplify enormously on the complex Sturmian basis set, and this allows us to calculate[10,18] partial rates for high-order ionization and harmonic generation by weak fields at short and long wavelengths.

The exact state vector $|\Psi_i(t)\rangle$ representing an electron initially bound in state i, satisfies the time-dependent Schrödinger equation

$$\left[i\hbar\frac{d}{dt}-H_a-V(t)\right]|\Psi(t)\rangle=0\ , \tag{1.1}$$

where H_a is the atomic Hamiltonian and $V(t)$ is the interaction of the electron with a field of frequency ω. We use the "velocity" gauge, with $V(t)=-(e/\mu c)\mathbf{A}(t)\cdot\mathbf{p}$, where e and μ are the electron charge and reduced mass, $\mathbf{p}$ is the canonical momentum operator for the electron, and $\mathbf{A}(t)$ is the (spatially independent) vector potential for the field; we have removed the $A(t)^2$ term by a simple gauge transformation. To pass to a time-independent theory we make the Floquet ansatz.[13,17] Thus we put

$$|\Psi_i(t)\rangle\simeq\exp(-i\varepsilon_i t/\hbar)|\psi_i(\tau)\rangle\ , \tag{1.2}$$

where $|\psi_i(\tau)\rangle$ is periodic in $\tau=\omega t$, with period 2π, and where ε_i is the electron quasienergy. Substituting the right-hand side of Eq. (1.2) into (1.1) we obtain

$$\left[i\hbar\frac{d}{dt}+\varepsilon_i-H_a-V(t)\right]|\psi_i(\tau)\rangle=0\ . \tag{1.3}$$

If we make the Fourier expansion

$$|\psi_i(\tau)\rangle=\sum_n e^{-in\tau}|\psi_{in}\rangle\ , \tag{1.4}$$

and decompose $V(t)$ as

$$V(t)=V_+e^{-i\omega t}+V_-e^{i\omega t}\ , \tag{1.5}$$

we see that the harmonic components $|\psi_{in}\rangle$ satisfy the time-independent coupled equations

$$(\varepsilon_i+n\hbar\omega-H_a)|\psi_{in}\rangle=V_+|\psi_{i,n-1}\rangle+V_-|\psi_{i,n+1}\rangle\ . \tag{1.6}$$

The solutions of Eqs. (1.6) are constrained by physically appropriate boundary conditions in coordinate space, namely, if $\mathbf{x}$ denotes the electron coordinate, and if $r=|\mathbf{x}|$, each harmonic component $\langle\mathbf{x}|\psi_{in}\rangle$ is regular at $r=0$ and behaves as a superposition of outgoing waves for $r\sim\infty$:

$$\langle\mathbf{x}|\psi_{in}\rangle\sim\sum_m f_{mn}(\varepsilon_i,\hat{\mathbf{x}})r^{i\nu_m}\exp(ik_{im}r)/r\ ,\quad r\sim\infty \tag{1.7}$$

where

$$k_{im}=[(2\mu/\hbar^2)(\varepsilon_i+m\hbar\omega)]^{1/2}\ , \tag{1.8}$$

and where $\nu_m=Z/(a_0k_{im})$, with $-Ze$ the charge of the residual ion. The homogeneous system of equations, (1.6), together with these boundary conditions, form an eigenvalue problem for ε_i. In solving these equations we exploit the fact that the harmonic components $|\psi_{in}\rangle$ are coupled together in *tridiagonal* form, a property which also holds in the length gauge[1] but not in the acceleration gauge.[4]

The eigenvalue is, of course, complex:

$$\varepsilon_i=E_i+\Delta_i-i\Gamma_i/2\ , \tag{1.9}$$

where Δ_i is the shift from the unperturbed energy E_i, and Γ_i is the induced width. The presence of the imaginary part of ε_i means that, while $\exp(-i\varepsilon_i t/\hbar)$ decays as t increases, $\langle\mathbf{x}|\psi_{in}\rangle$ explodes exponentially as r increases since $\mathrm{Im}(k_{im})<0$ if $m\geq N_0$, where N_0 is the minimum value of n for which $E_i+\Delta_i+n\hbar\omega>0$. Consequently, the cycle-averaged overlap

$$\frac{1}{2\pi}\int_0^{2\pi}d\tau\langle\psi_i(\tau)|\psi_i(\tau)\rangle=\sum_n\langle\psi_{in}|\psi_{in}\rangle \tag{1.10}$$

does not formally exist, except in the limit where the intensity I vanishes. In fact, as discussed in Appendix A, $\sum_n\langle\psi_{in}|\psi_{in}\rangle$ jumps discontinuously from 1 to 2 as I increases from zero to an infinitesimal but positive value. This is a consequence of passing to a time-independent framework, within which the field is of constant intensity and persists for all time so that even an infinitesimally weak field ionizes the atom.

In the next section we derive an expression for the harmonic-generation rate in terms of the expectation value $\mathbf{d}(t)$ of the atomic dipole moment with respect to the Floquet state vector $|\psi_i(\tau)\rangle$. We expand $\mathbf{d}(t)$ in a Fourier series, with components $\mathbf{d}_N\exp(-iN\omega t)$, where $\mathbf{d}_N$ is the complex dipole moment which generates photons of frequency $N\omega$. We express $\mathbf{d}_N$, which depends on the normalization of $|\psi_i(\tau)\rangle$, as a sum of subterms $\mathbf{d}_{Nn}$, which result from the expansion of $|\psi_i(\tau)\rangle$ in terms of its harmonic components, cf. Eq. (1.4) above. Each $\mathbf{d}_{Nn}$ is (nearly) divergent, but in Appendix B we show that the divergences cancel in the sum $\mathbf{d}_N$. We also consider, in Appendix B, the effect of a gauge transformation of the field, and indicate how the boundary condition (1.7) should be modified. This boundary condition is correct in the velocity gauge but not in the length gauge. This is because in the latter gauge $V(t)$ diverges for $r\sim\infty$. [In the velocity gauge $V(t)$ diverges for $p\sim\infty$, but this divergence is swamped by the kinetic energy, $\mathbf{p}^2/2\mu$.] Moreover, we show that while the $\mathbf{d}_{Nn}$ are not separately gauge invariant, the sum $\mathbf{d}_N$ is.

In Sec. III we discuss our results. In Appendix A we discuss the (analytic continuation of the) overlap X_{ji} of two Floquet state vectors $|\psi_i(\tau)\rangle$ and $|\psi_j(\tau)\rangle$. We show that X_{ji} is zero if $\varepsilon_i\neq\varepsilon_j$. However, X_{ii}, the quantity appearing on both sides of Eq. (1.10) above, is a discontinuous function of I at $I=0$, for a field of infinite duration. The overlap $X_{\bar{j}i}^T$ of $|\psi_i(\tau)\rangle$ and $T|\bar{\psi}_j(-\tau)\rangle$, where T is the time-reversal operator, and where the bar indicates that the sense of the field polarization has been reversed, is also zero if $\varepsilon_i\neq\varepsilon_j$. If $\bar{i}$ denotes the state obtained from i by reversing the sign of the electronic angular momenta, $X_{\bar{i}i}^T$ is continuous at $I=0$, and may be set equal to unity for all I; this provides a convenient prescription for normalizing $|\psi_i(\tau)\rangle$. In Appendix C we present formulas which are useful in discussing the case of an intermediate resonance in multiphoton ionization. Near a resonance the real parts of two Floquet eigenvalues approach one another. Whether the eigenvalues exhibit a true or avoided crossing, as the resonance is passed, is determined by

whether the two-valued complex Rabi frequency stays on the same branch or switches branches, respectively.

II. HARMONIC GENERATION: FORMAL EXPRESSIONS

When a laser beam passes through a medium it induces an oscillating dipole moment in each atom in the path of the beam. A dipole moment $\mathrm{Re}(\mathbf{D}e^{-i\Omega t})$, oscillating at frequency Ω, generates electric and magnetic fields, $\mathrm{Re}[\mathbf{E}(\mathbf{x})e^{-i\Omega t}]$ and $\mathrm{Re}[\mathbf{B}(\mathbf{x})e^{-i\Omega t}]$, respectively, which are given in the radiation zone by[19] $\mathbf{B}(\mathbf{x})=(\hat{\mathbf{n}}\times\mathbf{D})F(r)$ and $\mathbf{E}(\mathbf{x})=\mathbf{B}(\mathbf{x})\times\hat{\mathbf{n}}$, where

$$F(r)=(\Omega/c)^2\exp(i\Omega r/c)/r$$

and where $\hat{\mathbf{n}}$ is a unit vector which points along the direction of $\mathbf{x}$, that is, along the direction of observation. Both $\mathbf{E}(\mathbf{x})$ and $\mathbf{B}(\mathbf{x})$ lie in a plane, the polarization plane, which is perpendicular to $\hat{\mathbf{n}}$. We introduce two independent unit polarization vectors:

$$\hat{\boldsymbol{\varepsilon}}_1=\cos(\xi/2)\hat{\mathbf{x}}+i\sin(\xi/2)\hat{\mathbf{y}}\ , \tag{2.1a}$$

$$\hat{\boldsymbol{\varepsilon}}_2=\sin(\xi/2)\hat{\mathbf{x}}-i\cos(\xi/2)\hat{\mathbf{y}}\ , \tag{2.1b}$$

where the unit vectors $\hat{\mathbf{x}}$ and $\hat{\mathbf{y}}$ define the polarization plane, and where the retardation angle ξ may have a value ranging from 0 (linear polarization) to $\pi/2$ (circular polarization). The complex-conjugate vectors $\hat{\boldsymbol{\varepsilon}}_1^*$ and $\hat{\boldsymbol{\varepsilon}}_2^*$ describe the opposite rotational sense of polarization from $\hat{\boldsymbol{\varepsilon}}_1$ and $\hat{\boldsymbol{\varepsilon}}_2$. We may easily verify the following useful properties of the polarization vectors:

$$\hat{\boldsymbol{\varepsilon}}_j^*\cdot\hat{\boldsymbol{\varepsilon}}_k=\delta_{jk}\ , \tag{2.2a}$$

$$\hat{\mathbf{n}}\times\hat{\boldsymbol{\varepsilon}}_j=(-1)^j i\hat{\boldsymbol{\varepsilon}}_k^*,\quad j\neq k \tag{2.2b}$$

$$\hat{\boldsymbol{\varepsilon}}_j\times\hat{\boldsymbol{\varepsilon}}_j=0\ , \tag{2.2c}$$

$$\hat{\boldsymbol{\varepsilon}}_1\times\hat{\boldsymbol{\varepsilon}}_2=-i\hat{\mathbf{n}}\ . \tag{2.2d}$$

In addition, we have, of course, $\hat{\mathbf{n}}\cdot\hat{\boldsymbol{\varepsilon}}_j=0$. If we expand $\mathbf{D}$ as

$$\mathbf{D}=D_1\hat{\boldsymbol{\varepsilon}}_1+D_2\hat{\boldsymbol{\varepsilon}}_2+D_3\hat{\mathbf{n}}\ , \tag{2.3}$$

and use Eq. (2.2b), we obtain, for $j=1,2$, the components $B_j(\mathbf{x})$ of $\mathbf{B}(\mathbf{x})$ along $\hat{\boldsymbol{\varepsilon}}_j^*$, and the components $E_j(\mathbf{x})$ of $\mathbf{E}(\mathbf{x})$ along $\hat{\boldsymbol{\varepsilon}}_j$; we have $B_k(\mathbf{x})=i(-1)^j D_j F(r)$, $j\neq k$, and $E_j(\mathbf{x})=D_j F(r)$, for $j,k=1,2$. The power radiated into the solid angle $d\hat{\mathbf{n}}$ is

$$\begin{aligned}dW/d\hat{\mathbf{n}}&=(c/8\pi)r^2\hat{\mathbf{n}}\cdot[\mathbf{E}(\mathbf{x})\times\mathbf{B}^*(\mathbf{x})]\\&=(c/8\pi)(\Omega/c)^4(|D_1|^2+|D_2|^2)\ ,\end{aligned} \tag{2.4}$$

where in the second step we used Eqs. (2.2c) and (2.2d). The rate for emitting photons of frequency Ω into $d\hat{\mathbf{n}}$ is $(1/\hbar\Omega)dW/d\hat{\mathbf{n}}$. Since $D_j=\hat{\boldsymbol{\varepsilon}}_j^*\cdot\mathbf{D}$, the rate of (spontaneous) emission of photons with a specific polarization $\hat{\boldsymbol{\varepsilon}}$ is

$$\frac{dR(\Omega,\hat{\boldsymbol{\varepsilon}})}{d\hat{\mathbf{n}}}=\frac{\Omega^3}{8\pi\hbar c^3}|\hat{\boldsymbol{\varepsilon}}^*\cdot\mathbf{D}|^2\ . \tag{2.5}$$

The real atomic quantum-mechanical dipole moment induced by the laser field is

$$\mathbf{d}(t)=\langle\Psi_i(t)|e\mathbf{x}|\Psi_i(t)\rangle\ , \tag{2.6}$$

where e is the electron charge. If we make the Floquet ansatz, we obtain

$$\begin{aligned}\mathbf{d}(t)&\simeq\langle\psi_i(\tau)|e\mathbf{x}|\psi_i(\tau)\rangle e^{-\Gamma_i t/\hbar}\\&=e^{-\Gamma_i t/\hbar}\left[\mathbf{d}_0+\sum_{N>0}\mathrm{Re}(2\mathbf{d}_N e^{-iN\omega t})\right]\ ,\end{aligned} \tag{2.7}$$

where in the second step we used Eq. (1.4) and we defined

$$\mathbf{d}_N=\sum_n\mathbf{d}_{Nn}\ , \tag{2.8a}$$

$$\mathbf{d}_{Nn}=\langle\psi_{i,n-N}|e\mathbf{x}|\psi_{in}\rangle\ , \tag{2.8b}$$

noting that since $\mathbf{d}(t)$ is real we have $\mathbf{d}_{-N}=\mathbf{d}_N^*$. The rate for generating photons of frequency $\Omega=N\omega$ and polarization $\hat{\boldsymbol{\varepsilon}}$ is given by putting $\mathbf{D}=2\mathbf{d}_N$ in Eq. (2.5). Note that $\mathbf{d}_N$ depends on the normalization of $|\psi_i(\tau)\rangle$. If the state i has a definite parity, $\sigma(=\pm1)$ say, the function $\langle\mathbf{x}|\psi_{i,m}\rangle$ has parity $\sigma(-1)^m$ since $|\psi_{i,m}\rangle$ represents an electron which has absorbed m (real or virtual) photons, each of parity (-1). Hence $\langle\psi_{i,n-N}|\mathbf{x}\rangle\langle\mathbf{x}|\psi_{in}\rangle$ has parity

$$\sigma(-1)^{n-N}(-1)^n\sigma=(-1)^N\ ,$$

and therefore $\mathbf{d}_{Nn}$, and $\mathbf{d}_N$, vanish unless N is odd. In the weak-field limit $|\psi_{im}\rangle$ is of order $I^{|m/2|}$ and so $\mathbf{d}_{Nn}$ is of order $I^{|N-n|/2}I^{|n/2|}$, that is, of order $I^{N/2}$ if $0\le n\le N$, and of higher order if n is outside this range. Consequently, within perturbation theory the summation index in Eq. (2.8a) runs only over 0 to N. At intensities beyond the weak-field limit, each $\mathbf{d}_{Nn}$ has a near divergence, but these near divergences cancel in the sum, as we discuss in Appendix B.

III. RESULTS

We solved Eqs. (1.6) by expanding the harmonic components $|\psi_{in}\rangle$ in terms of Sturmian basis functions $S_{ml}^{\kappa}(r)$ which oscillate as $r^m\exp(i\kappa r)$ for $r\sim\infty$, where the wave number κ was chosen to lie in the upper right quadrant of the complex κ plane. The rate of convergence with respect to the number of basis functions is sensitive to the choice of κ; we have discussed this in detail elsewhere.[3,18] By using the orthornormality relation

$$\int_0^\infty dr\, S_{m'l}^{\kappa}(r)(1/r)S_{ml}^{\kappa}(r)=\delta_{mm'}\ , \tag{3.1}$$

we obtained a set of homogeneous linear equations for the coefficients of the basis functions. These equations were solved, for both the eigenvalue and the coefficients, by using the method of inverse iteration.[13]

In a previous paper[15] we discussed the ionization of H(1s) by linearly polarized light of wavelength 355 nm within the truncated threshold approximation (TTA). In the TTA the harmonic expansion of a Floquet state vector is truncated at the term $n=N_0-1$, that is, just below the continuum threshold. The exclusion of harmonic components corresponding to absorption above threshold means that the widths vanish and hence that the eigenvalues are real. We calculated, within the TTA, the 1s

and $2p$ eigenvalues at various intensities, and we found that they exhibited an avoided crossing corresponding to an intermediate resonance of the three-photon $1s \rightarrow 2p$ transition. The gap between the eigenvalue curves at resonance is just the coupling energy $\hbar\Omega_0$ between the $1s$ and $2p$ states, where Ω_0 is the Rabi frequency for the $1s \rightarrow 2p$ transition. We have now recalculated the $1s$ and $2p$ eigenvalue curves, this time including harmonic components corresponding to absorption above threshold; we included a sufficient number of harmonic components to ensure convergence of the eigenvalues. In Fig. 1 we show $\mathrm{Re}(\varepsilon_{1s})$ and $\mathrm{Re}(\varepsilon_{2p})-3\hbar\omega$ versus intensity I. We also show the widths Γ_{1s} and Γ_{2p}. In contrast to what we found earlier, we now see a true crossing rather than an avoided crossing of the real parts of the eigenvalues. The reason for this is that, at the intensity where the crossing occurs, Γ_{1s} is very small while Γ_{2p} is larger than $\hbar\Omega_0$. The fact that a true crossing occurs when the difference of the widths of the eigenvalues exceeds $\hbar\Omega_0$ (that is, when the difference of the couplings of the bare atomic states to the continuum exceeds the coupling between the states) has been discussed previously by Gontier and Trahin,[20] and by Holt *et al.*,[21] and in Appendix C we summarize part of their analysis. Surprisingly, Γ_{1s} shows no enhancement at resonance; we might expect the $1s \rightarrow 2p$ excitation rate to peak at resonance, and Γ_{1s} to peak accordingly. In fact, however, the $1s \rightarrow 2p$ excitation rate does not peak when the intensity is varied around the value I_r where the detuning, $\delta\omega$, from resonance vanishes. To understand this, note first that the energy shifts, and therefore $\delta\omega$, vary linearly with I, at least to lowest order in I; we have $\delta\omega \simeq \alpha(I - I_r)$ where α is constant. Note further that if γ_{2p} denotes the rate of decay of the $2p$ state in the absence of coupling to the $1s$ state, γ_{2p} also varies linearly with I since only one 355-nm photon need be absorbed to ionize the atom in the $2p$ state; $\gamma_{2p} \simeq \beta I$, with β a constant. Referring to Eq. (C12d) for the excitation rate, $\gamma_{\mathrm{ex}}(\delta\omega)$, from state $i \equiv 1s$ to $j \equiv 2p$, and noting that $\gamma_i \equiv \gamma_{1s} \ll \gamma_j \equiv \gamma_{2p}$, we see that the denominator on the right-hand side of Eq. (C12d) is roughly $\alpha^2(I - I_r)^2 + \beta^2 I^2$. This denominator has a minimum at $I = \alpha^2 I_r/(\alpha^2 + \beta^2)$ which differs significantly from I_r since, in the present case, β is not negligible (from Fig. 1 we may infer that roughly $\beta \simeq \alpha/2$); hence $\gamma_{\mathrm{ex}}(\delta\omega)$ does not peak as I passes through the resonance intensity I_r where $\delta\omega = 0$. In Fig. 2 we show $\mathrm{Re}(\varepsilon_{1s})$ and $\mathrm{Re}(\varepsilon_{2p})-3\hbar\omega$, as well as the widths, versus frequency ω, with the intensity fixed at the value 1.15×10^{13} W/cm^2 at which the crossing in Fig. 1 occurs. We now see an enhancement of Γ_{1s} at resonance because γ_i and γ_j vary very slowly with ω and the denominator on the right-hand side of Eq. (C12d) exhibits a minimum as ω is varied around the resonance frequency.

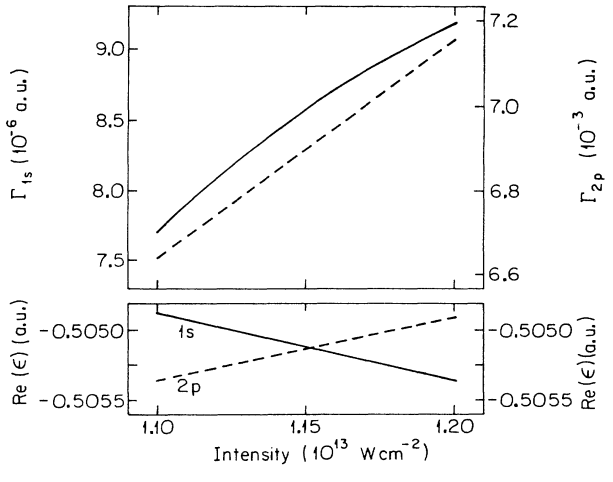

FIG. 1. Widths of ε_{1s} and ε_{2p} (upper curves) and real parts of ε_{1s} and $\varepsilon_{2p}-3\hbar\omega$ (lower curves) vs intensity, for hydrogen irradiated by linearly polarized light of wavelength 355 nm. Solid and dashed curves correspond to states which are the $1s$ and $2p$ states, respectively, in the weak-field limit.

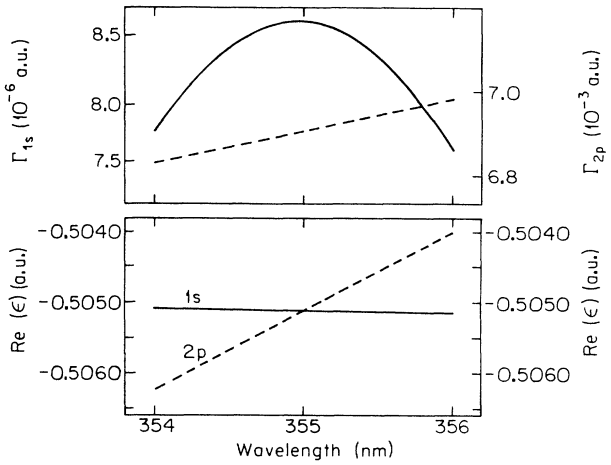

FIG. 2. Same as Fig. 1 but vs frequency, with the intensity fixed at 1.151×10^{13} W/cm^2. The crossing occurs at the wavelength 355 nm.

In Ref. 15 we also used the TTA to study the ionization of H($1s$) by linearly polarized light of wavelength 204 nm. There is an intermediate two-photon $1s \rightarrow 3s$ resonance, and within the TTA we found an avoided crossing between ε_{1s} and $\varepsilon_{3s}-2\hbar\omega$ corresponding to this resonance. We have redone this calculation, now without truncation at threshold, and we still find an avoided crossing. In this instance the difference of the widths is smaller than $\hbar\Omega_0$, where here Ω_0 denotes the Rabi frequency of the $1s \rightarrow 3s$ transition.

In Fig. 3 we show the real parts of 27 different eigenvalue curves versus intensity I for linearly polarized light of wavelength 1064 nm. All of the eigenvalues shown correspond to states which have parity $(-1)^{N_j}$ and which, for $I \sim 0$, are detuned from an N_j-photon resonance with the $1s$ state by no more than $\hbar\omega$. As in Fig. 1, we display $\mathrm{Re}(\varepsilon_j)-N_j\hbar\omega$ rather than ε_j. (Note that if ε_j is an eigenvalue, so is $\varepsilon_j + m\hbar\omega$ for any integer m. We specify ε_j uniquely by requiring that $\varepsilon_j \rightarrow E_j$, and hence $|\psi_{jm}\rangle \rightarrow |\Phi_j\rangle\delta_{mo}$, as $I \rightarrow 0$, where $|\Phi_j\rangle$ represents the unperturbed bound state j.) Here we label ε_j by an integer index j which corresponds to the order in which

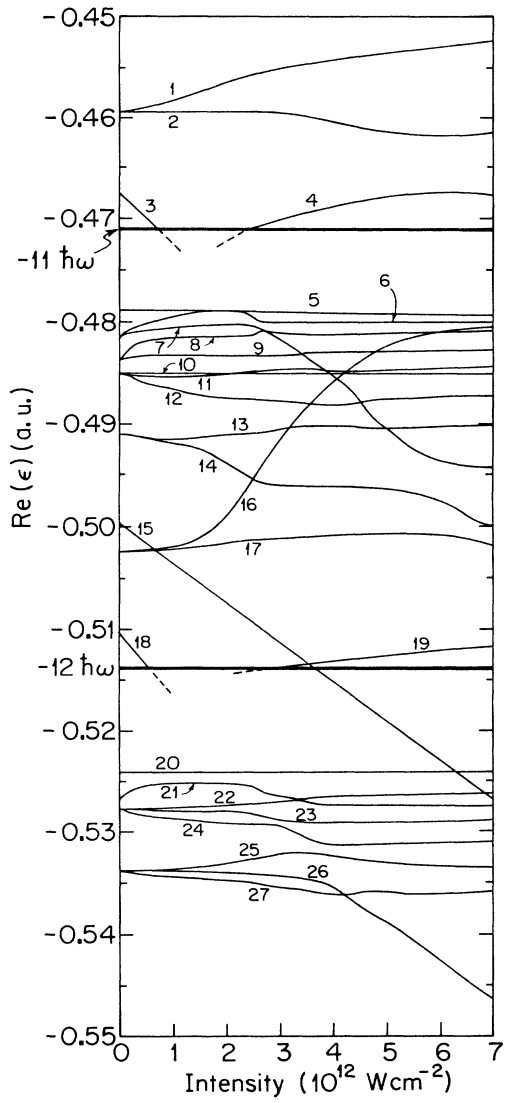

FIG. 3. Real parts of various eigenvalues ε_j for hydrogen irradiated by linearly polarized light of wavelength 1064 nm. We show $\mathrm{Re}(\varepsilon_j)-N_j\hbar\omega$, where the integer index j labels the following atomic configurations (or superpositions of configurations), where known, in the weak-intensity limit. (1–2): superpositions of $4s$ and $4d$, $N_{1-2}=10$; (3): $2s$, $N_3=8$; (4): unknown; (5): superposition of $8p$, $8f$, $8h$, and $8j$, $N_5=11$; (6–7): superpositions of $7p$, $7f$, and $7h$, $N_{6-7}=11$; (8–9): superpositions of $3s$ and $3d$, $N_{8-9}=10$; (10–12): superpositions of $6p$, $6f$, and $6h$, $N_{10-12}=11$; (13–14): superpositions of $5p$ and $5f$, $N_{13-14}=11$; (15): $1s$, $N_{15}=0$; (16–17): superpositions of $4p$ and $4f$; $N_{16-17}=11$; (18): $2p$, $N_{18}=9$; (19): unknown; (20): superposition of $7s$, $7d$, $7g$, and $7i$, $N_{20}=12$; (21): $3p$, $N_{21}=11$; (22–24): superpositions of $6s$, $6d$, and $6g$, $N_{22-24}=12$; (25–27): superpositions of $5s$, $5d$, and $5g$, $N_{25-27}=12$. We did not include states with orbital angular momentum quantum number greater than 7. The bold horizontal lines indicate multiphoton ionization thresholds. Note that reduced mass effects are included, so that, for example, $\mathrm{Re}(\varepsilon_{15})$ approaches a value slightly above -0.5 a.u. in the zero-intensity limit.

$\mathrm{Re}(\varepsilon_j)-N_j\hbar\omega$ appears in Fig. 3. However, when no confusion might arise we refer to $\varepsilon_j-N_j\hbar\omega$ simply as ε_j, and we do not distinguish between ε_j and $\mathrm{Re}(\varepsilon_j)$. Thus, for example, ε_{18}, the eigenvalue corresponding to the $2p$ state when $I\sim 0$, is displayed as $\varepsilon_{18}-9\hbar\omega$ and appears below ε_{15}, the eigenvalue corresponding to the $1s$ state ($N_{15}=0$). We show all of those eigenvalues corresponding to atomic states with principal quantum number ≤ 6 when $I\sim 0$, and a few more besides. In the zero-field limit the eigenvectors are, in general, superpositions of atomic states with the same principal quantum number and parity, but different orbital angular momentum quantum numbers.[15] We note that absorption of twelve 1064-nm photons is required for weak-field ionization from the $1s$ state, three photons from the $n=2$ states, two photons from the $n=3$ states, and only one photon from all states with principal quantum number $n\geq 4$.

We calculated[22] these eigenvalues within the velocity gauge, with the A^2 term subtracted so that the continuum threshold does not shift. Thus we might expect the shifts of the high Rydberg states to be small. This is indeed the case for many of these states; see, for example, ε_5, ε_{8-11}, ε_{17}, ε_{20}, and ε_{22}, which stay rather flat as I varies. However, some of the Rydberg states undergo large shifts, often because of strong coupling to the $2s$ or $2p$ states. For example, as I increases, ε_3, the eigenvalue originating from the $2s$ level, shifts downwards by roughly the ponderomotive energy P and passes below a multiphoton ionization threshold at about 0.7×10^{12} W/cm^2. (The number of 1064-nm photons required to ionize an atom which is initially in the $2s$ state increases from 3 to 4 as this threshold is passed.) Not far below the threshold, ε_3 undergoes an avoided crossing with an eigenvalue curve originating from a very high Rydberg level. We do not know which Rydberg level this is; in fact, we cannot precisely calculate the eigenvalues just below a multiphoton ionization threshold because an infinite number of Rydberg states accumulate there and give rise to a myriad of true and avoided crossings. However, when two eigenvalue curves undergo an avoided crossing, the characters of the corresponding Floquet states interchange (see Appendix C). Thus, at the first avoided crossing encountered by ε_3, the other curve (which originates from a very high Rydberg level) acquires $2s$ character, and at intensities above the crossing intensity this second curve shifts downwards until (almost immediately) it encounters an avoided crossing with another curve originating from a high Rydberg level, and so on. In Fig. 3, the eigenvalue ε_6, which originates from a level with principal quantum number 7, has a noticeable bend at $I\simeq 2.3\times 10^{12}$ W/cm^2 which in fact signifies almost simultaneous avoided crossings with a curve (not shown in Fig. 3) originating from a higher Rydberg level, and with ε_7, another curve originating from a level with principal quantum number 7. The $2s$ character acquired by ε_6 is almost immediately transferred to ε_7 as I increases, and ε_7 shifts downwards without interruption as it undergoes true crossings with ε_{8-13}, until the avoided crossing with ε_{14}. One can easily trace, through the avoided crossings, the diabatic curve which at each intensity (far from a

crossing) corresponds to the Floquet state which has predominantly $2s$ character. This diabatic curve is (more or less) the straight line $E_{2s}-8\hbar\omega-P$ where P, the ponderomotive shift, is proportional to I ($P=2\pi e^2 I/\mu c\omega^2$). Similarly, the diabatic curve which corresponds to the Floquet state that is predominantly $2p$ in character starts as ε_{18}, but after passing through many avoided crossings becomes ε_{26}; it is approximately $E_{2p}-9\hbar\omega-P$. We remark that the diabatic "$2s$" and "$2p$" curves are nearly parallel to ε_{15}, the "$1s$" curve, and do not cross it until the intensity becomes fairly large.

The eigenvalues ε_4 and ε_{19} are rather interesting because they each cross a multiphoton ionization threshold from *below* to *above* as the intensity increases. Unfortunately, our finite basis set does not allow us the accuracy to ascertain the zero-field limits of these curves. The thresholds crossed by ε_4 and ε_{19} would be *zero*-photon ionization thresholds if these curves were to originate from a level with a principal quantum number greater than 3 (from which ionization can occur by absorption of only one photon). However, this would be physically uninteresting. At a given intensity, the scattering matrix has a resonance pole at each eigenvalue, and the dynamics of the ionization process is governed by those poles which lie close to the physical energy axis. If a pole which originates as a bound-state pole were to pass the zero-photon ionization threshold it would move farther away from the physical energy axis, and therefore cease to be physically significant.[16] Our analysis of the stability[16] of the eigenvalues ε_4 and ε_{19} strongly suggests, in fact, that the corresponding poles lie *close* to the physical energy axis (i.e., they can be reached from this axis by paths which do not encircle a threshold), as soon as they cross the threshold upwards: perhaps curves 3 and 4 are sections of the same adiabatic curve, as perhaps 18 and 19 are, or perhaps the poles 4 and 19 are stray "shadow" poles[16] at intensities below the threshold intensity, but they become "dominant" poles at intensities above the threshold.[23] We refer the reader to an earlier paper[16] for a fuller account of the movement of resonance poles in strong oscillating fields.

At $I=3.5\times10^{12}$ W/cm^2, the widths of the states shown in Fig. 3 are typically of order 10^{-4} or 10^{-3} a.u., with the exceptions of ε_{15} ($\Gamma_{15}\approx10^{-16}$ a.u. at this intensity), ε_5 ($\Gamma_5=8\times10^{-9}$ a.u.), ε_{20} ($\Gamma_{20}=2.5\times10^{-6}$ a.u.), ε_{10} ($\Gamma_{10}\simeq4\times10^{-5}$ a.u.), and ε_{16} ($\Gamma_{16}\simeq2.5\times10^{-2}$ a.u.). At all intensities below 7×10^{12} W/cm^2, the states 5, 20, and 10 are predominantly $8j$, $7i$, and $6h$ atomic states, respectively, i.e., highly excited states of maximum angular momentum. The ionization rates of these states are particularly small and the real parts of their eigenvalues do not exhibit any appreciable shift, since they are very diffuse and couple weakly to the field. In addition, there is a Floquet state, 5′ say, not shown in Fig. 3, which is predominantly $8h$ in character; $\mathrm{Re}(\varepsilon_{5'})$ is nearly identical to $\mathrm{Re}(\varepsilon_5)$ at all intensities below 7×10^{12} W/cm^2, but $\Gamma_{5'}$ is much larger than Γ_5, e.g., $\Gamma_{5'}=3.8\times10^{-5}$ a.u. at $I=3.5\times10^{12}$ W/cm^2. (Like the other Floquet states, ε_5, $\varepsilon_{5'}$, ε_{10}, and ε_{20} are actually superpositions of several atomic states, dominated, however, by a particular one, in proportions that vary with the field strength; therefore, their widths increase more rapidly with the intensity than the linear power law expected for single Rydberg states in weak fields.) On the other hand, we see that ε_{16} exhibits a very large shift and width, indicating strong coupling to the field. This is presumably related to the fact that ε_{16} has a $4p$ character at small intensities [of all unperturbed atomic states, it is the $4p$ that has the largest ionization rate in the weak-field limit, since the states with principal quantum number $n<4$ require at least two 1064-nm photons to be ionized, and the rates for ionization from H(nl) decrease with increasing n or l for $n\geq4$].

We now focus on ε_{15}, the eigenvalue in Fig. 3 which corresponds to the $1s$ state when $I\sim0$. We see that $\mathrm{Re}(\varepsilon_{15})$ exhibits numerous true crossings, but apparently no avoided crossings with other eigenvalue curves. Apparently, at resonances between states 15 and j the difference of the "uncoupled" widths γ_{15} and γ_j is larger than $\hbar\Omega_0$. Since a large number of 1064-nm photons is required to either ionize H($1s$) or (on resonance) excite H($1s$) to state j, the width γ_{15} and (on resonance) the Rabi frequency Ω_0 are both very small, while since few photons are required to ionize the atom from an excited state j the width γ_j is relatively large, at least if j is not too highly excited. Actually, if j corresponds to a high Rydberg level with principal quantum number n, we have that in the weak-field limit Ω_0 and γ_j decrease with increasing n (fixed l) as $n^{-3/2}$ and n^{-3}, respectively (since the probability for the electron to be near the nucleus decreases as n^{-3} with increasing n); hence there may exist large (but not too large) n for which γ_{15} is substantially larger than γ_j but substantially smaller[24] than Ω_0, in which case avoided crossings will occur. We detected no avoided crossings for ε_{15}, although it is not possible to distinguish a true crossing from an avoided crossing with a very small gap, and perhaps some of the crossings are avoided, a point we return to below. Of course, for $n\sim\infty$ both Ω_0 and γ_j vanish and so $\mathrm{Re}(\varepsilon_{15})$ exhibits only true crossings immediately below a multiphoton ionization threshold. All said and done, $\mathrm{Re}(\varepsilon_{15})$ barely differs from the diabatic curve, which to an excellent approximation is $E_{1s}-1.0084P$ for intensities below 3×10^{13} W/cm^2. Hence an electron which starts in the $1s$ state will remain on the diabatic eigenvalue curve; the coupling to other Floquet states, at true crossings, is small, and the electron will simply jump across the gap of an avoided crossing if this gap is very small.[15] Therefore ionization from H($1s$) at long wavelengths (e.g., 1064 nm), by a pulse whose intensity envelope $I(t)$ varies slowly on the time scale of a cycle, can be described by the width of a single eigenvalue. The total ionization probability is $1-\exp(-\int dt\,\Gamma_i/\hbar)$, where the width Γ_i (with $i=15$) depends implicitly on t through $I(t)$, and where the integration limits are $\pm\infty$. In Fig. 4 we show $\Gamma_{15}/\hbar$ versus I over the range $5\times10^{12}\leq I\leq3\times10^{13}$ W/cm^2.[22] The resonance peaks of Γ_{15} correspond to crossings of $\mathrm{Re}(\varepsilon_{15})$ with other eigenvalue curves. The first group of resonances seen in Fig. 4 is associated with the group of crossings of $\mathrm{Re}(\varepsilon_{15})$ with $\mathrm{Re}(\varepsilon_j)$ (with

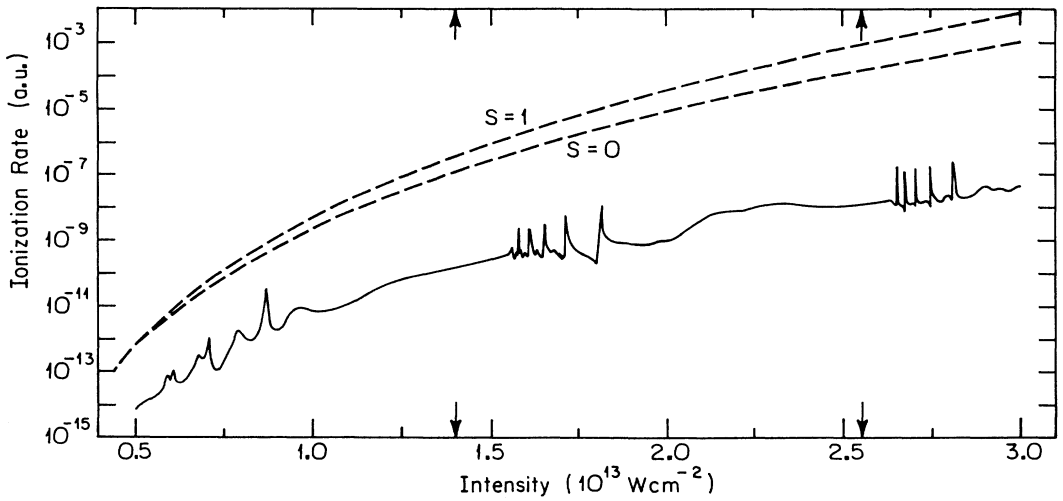

FIG. 4. Total ionization rate vs intensity for H(1s) irradiated by linearly polarized light of wavelength 1064 nm. Dashed curves are partial rates for $(12+S)$-photon ionization obtained within lowest-order perturbation theory. The arrows indicate the intensities at which the real part of the 1s Floquet eigenvalue crosses the 13- and 14-photon ionization thresholds.

$j=20-25$, 27, and 1) in the intensity range $6-10\times10^{12}$ W/cm^2. These resonances involve intermediate 11- or 12-photon transitions from the 1s state to highly excited states. Not all of the crossings lead to an enhancement of the width Γ_{15}, a feature we already saw in Fig. 1; for example, the crossing of $\mathrm{Re}(\varepsilon_{15})$ with $\mathrm{Re}(\varepsilon_{23})$ or $\mathrm{Re}(\varepsilon_{27})$ leads to no enhancement. An analysis of the presence or absence of resonance enhancement of the width is more difficult here (than was the case for Fig. 1) because the two-level model used in Appendix C is hardly adequate when one of the levels is a high Rydberg level—there are many other high Rydberg levels which are close by. Moreover, it might be that the resonance peaks occur mainly at avoided crossings, which must, however, have very small gaps since we detected none in Fig. 3. The middle group of resonances seen in Fig. 4 involves intermediate 12- or 13-photon transitions from the 1s state to excited states, corresponding to crossings occurring in the intensity range $1.5-2\times10^{13}$ W/cm^2 (not covered in Fig. 3) where $\mathrm{Re}(\varepsilon_{15})$ crosses the group of curves $\mathrm{Re}(\varepsilon_{5-14})$ and $\mathrm{Re}(\varepsilon_{16-17})$ when this group is displaced downwards by $2\hbar\omega$, that is, when N_j is increased by 2 for $j=5-14$ and 16–17. The third group of resonances, occurring in the intensity range $2.7-3\times10^{13}$ W/cm^2, is a replication, though an imperfect one, of the first group; thus if the $\mathrm{Re}(\varepsilon_j)$ of the first group are displaced downwards by $2\hbar\omega$ (that is, if N_j is increased by 2 for $j=20-25$, 27, and 1) this group is again crossed by $\mathrm{Re}(\varepsilon_{15})$, the crossings now corresponding to intermediate 13- or 14-photon resonant transitions to the excited states of the first group. Although $\mathrm{Re}(\varepsilon_{15})$ crosses many eigenvalue curves immediately below a multiphoton ionization threshold, the rate of excitation [$\gamma_{\mathrm{ex}}(\delta\omega)$ in Appendix C] to these very high Rydberg states is very small, and so Γ_{15} exhibits little or no enhancement immediately below a threshold. Note that within a group of resonances, the peaks are narrower at lower intensities. This can be understood if the peaks occur only at avoided crossings; for the width of a peak at an avoided crossing is proportional to the Rabi frequency Ω_0, at least within the two-level model—see Appendix C, Eqs. (C11b) and (C11c)—and resonances at lower intensity correspond to upper levels with higher principal quantum number and accordingly smaller Ω_0. Furthermore, comparing two different groups of resonances, the peaks in the group corresponding to the higher intensity are narrower, which we can

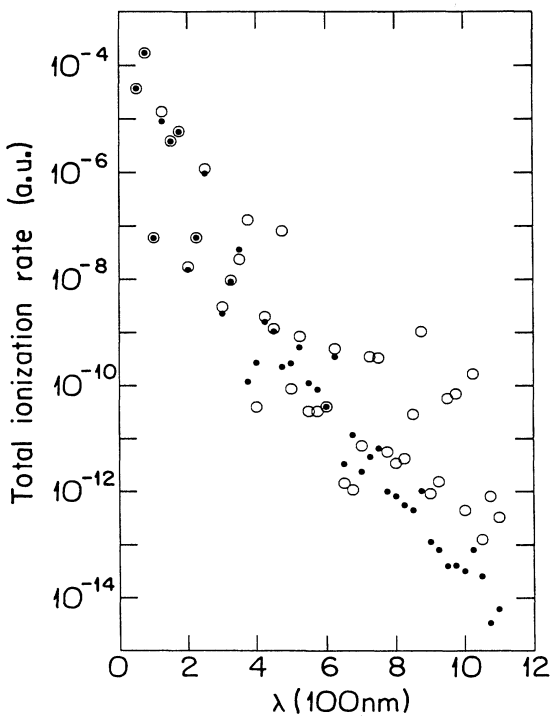

FIG. 5. Total rate for ionization of H(1s) by linearly polarized light, with the intensity fixed at 5×10^{12} W/cm^2, for wavelengths increasing from 50 to 1100 nm by steps of 25 nm. The dots represent the nonperturbative estimates; the circles represent the partial rate for ionization into the $S=0$ channel obtained within lowest-order perturbation theory.

again understand if the peaks occur at avoided crossings, because the resonances in the higher-intensity group involve more photons and Ω_0 is accordingly smaller.

We also show in Fig. 4 the partial ionization rates, calculated within lowest (nonvanishing) order *perturbation theory*, for (N_0+S)-photon ionization, with $N_0=12$ and $S=0$ and 1. The partial rates should sum to the total rate $\Gamma_{1S}/\hbar$, but clearly the partial rates, when calculated in perturbation theory, are grossly overestimated.[25] This overestimation of the perturbative rates is due to the neglect of both the increase in the ionization potential and the (oscillating) polarization of the atom (the effect of the latter is that the electron spends less time near the atomic nucleus where it can absorb photons). In Fig. 5 we show the behavior of the total ionization rate, $\Gamma_{1s}/\hbar$, versus wavelength, for a fixed intensity of 5×10^{12} W/cm^2. (The minimum number of photons required to ionize the atom, N_0, is roughly proportional to the wavelength, and varies from 1 at 50 and 75 nm to 13 at 1100 nm, in the weak-field limit. N_0 remains equal to its weak-field value at 5×10^{12} W/cm^2 for most wavelengths we consider in Fig. 5; however, one more photon has to be absorbed for ionizing the atom at 725, 900, 975, and 1075 nm.) We see that, on the average, Γ_{1s} diminishes rapidly as the wavelength increases, though there are fluctuations due to resonances. Perturbation theory yields a rate that is accurate at short wavelengths—except very close to resonances—that becomes inaccurate at longer wavelengths, and that is systematically too large at long wavelengths. (The ratio of the excursion amplitude to the atomic binding radius is $2.6\times10^{-12}I^{1/2}\lambda^2$, where I is the intensity in W/cm^2 and λ is the wavelength in nm; for $I=5\times10^{12}$ W/cm this parameter is 5.8×10^{-2} at $\lambda=100$ nm and 5.8 at $\lambda=1000$ nm. The ratio $P/\hbar\omega$ is about 0.4 at the same intensity and for $\lambda=1000$ nm.) In other words, the peak intensity below which perturbation theory is applicable decreases as the wavelength increases; above this peak intensity, and at long wavelengths, the nonperturbative total photoionization rates increase more slowly with the intensity than do the lowest-order perturbative rates.

Therefore perturbation theory predicts saturation intensities for long wavelengths which are much smaller than the nonperturbative estimates. As an example, we consider the probability for ionization of H(1s) by a 1064-nm, linearly polarized, Gaussian pulse $I(t)=I_0\exp(-t^2/t_p^2)$ with peak intensity $I_0=2\times10^{13}$ W/cm^2. Evaluating

$$1-\exp\left[-\int_{-\infty}^{t}dt'\Gamma_{1s}/\hbar\right],$$

assuming that the electron follows the diabatic curve, we find that if $t_p=100$ psec the fraction of atoms that has ionized at $t=0$, the peak intensity of the pulse, is roughly 0.2%, though replacing Γ_{1s} by the perturbative rate yields the result 99.99% (taking into account only the $S=0$ channel). We may ask what the maximum pulse duration should be if at least 10% of atoms are to experience the peak intensity of the pulse without being ionized; we find that t_p should be about 100 nsec, though perturbation theory (again taking into account only the $S=0$ channel) yields $t_p\simeq25$ psec.

In Fig. 6 we show the total ionization yield for H(1s) irradiated by a realistic pulse whose intensity distribution is (ρ and z are cylindrical coordinates)

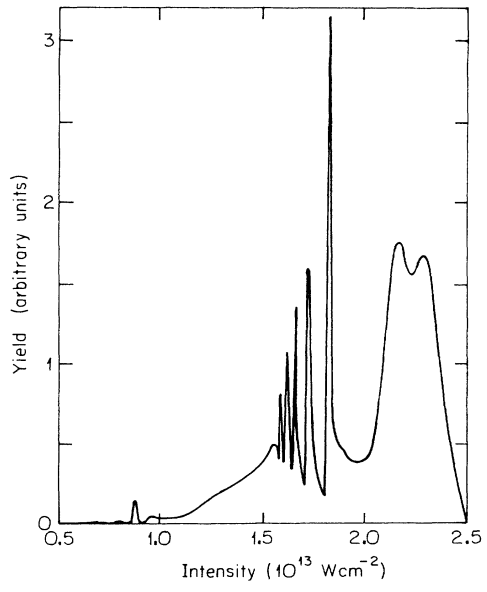

FIG. 6. Total ionization yield vs intensity for H(1s) irradiated by a pulse whose wavelength is 1064 nm, whose duration is 200 psec, whose focal spot size has a radius of 20 μm, and whose peak intensity is 2.5×10^{13} W/cm^2.

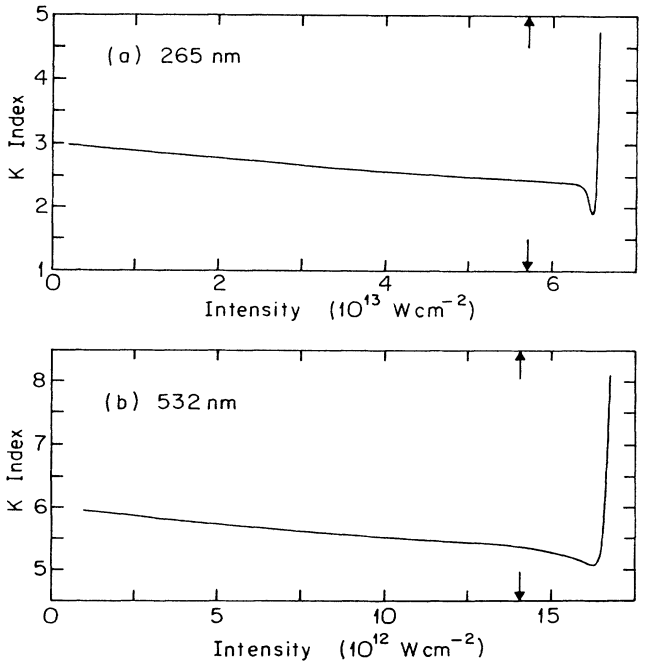

FIG. 7. Index of nonlinearity vs intensity for total ionization of H(1s) by linearly polarized light at wavelengths (a) 265 nm and (b) 532 nm. The arrows indicate the intensities at the first multiphoton ionization thresholds.

$$I(\rho,z,t)=[R^2/r^2(z)]I_0 e^{-2[\rho/r(z)]^2} e^{-t^2/t_p^2}, \quad (3.2)$$

where $t_p=200$ psec, where $I_0=2.5\times10^{13}$ W/cm^2, where $R=20$ μm is the spot size at the focus, and where, with the wavelength $\lambda=1064$ nm,

$$[r(z)]^2=R^2[1+(\lambda z/\pi R^2)^2] .$$

The figure represents the yield in ions as a function of the intensity at which they are produced, calculated from the nonperturbative rates of Fig. 4. We show the envelope of a histogram based on dividing the intensity interval $0\le I\le I_0$ into very small, equal segments. Variations in the pulse duration do not modify the results of Fig. 6, as long as t_p is not too large (saturation effects become apparent for $t_p>1$ ns) or too small (the system cannot be represented by a single Floquet state if the bandwidth of the laser is too large). Note that the yield vanishes at the peak intensity; this is because the spatial volume corresponding to the intensity segment in which the peak intensity occurs is proportional to the length dI of that segment, and therefore vanishes as dI vanishes. The resonance peaks are very prominent in the yield, and would remain prominent were we not to average over the spatial dimensions of the pulse. The contribution of these peaks, between $I=1.55\times10^{13}$ and 2×10^{13} W/cm^2, is about 30% of the total yield produced by the pulse; the (double) peak occurring at 2.0–2.5×10^{13} W/cm^2 arises from the shoulder seen in Fig. 4, and this provides most of the contribution to the remaining 70% of the yield. Since we have calculated the total yield, rather than the partial N-photon ionization yields, we cannot confirm the substructure seen in the peaks of the emergent electron energy distribution by Freeman *et al.*[26] However, our results do support the claim that levels shifting in and out of resonance strongly enhance the ionization yield. Recently, Cooke *et al.*[27] have made the interesting observation that in certain narrow regions of the laser focus, where the atoms experience a peak intensity which is equal to an intensity at which there is a resonance, ionization occurs with very high probability. This is borne out by our results.

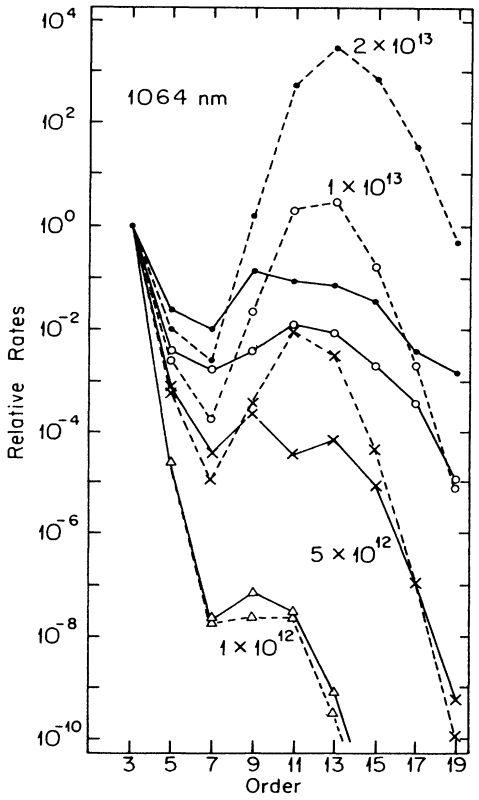

FIG. 8. Rates for harmonic generation of various orders by linearly polarized light of wavelength 1064 nm incident on H(1s). These rates are for emission into the direction of incident propagation, and are summed over polarizations of emitted light. We have normalized the rates to have the same value for the third harmonic. Dashed and solid curves are results obtained in lowest-order perturbation theory and our nonperturbative approximation, respectively, at the following intensities: —△—, 1×10^{12} W/cm^2; —×—, 5×10^{12} W/cm^2; —○—, 1×10^{13} W/cm^2; —●—, 2×10^{13} W/cm^2.

In Fig. 7 we present the index of nonlinearity, K, for the total ionization rate of H(1s) by linearly polarized light of wavelengths 265 or 532 nm. Here K is defined as the derivative of $\ln(\Gamma_{1s})$ with respect to $\ln(I)$. As I approaches zero, K approaches the perturbation-theory result N_0. However, K decreases as I increases, until a resonance is reached, when K shows sharp structure. The preliminary decrease[28] of K may seem surprising, particularly when the intensity passes a multiphoton ionization threshold, at which point N_0 increases by unity. Thus, for 265-nm light, N_0 jumps from 3 to 4 at about 5.7×10^{13} W/cm^2, and for 532-nm light, N_0 jumps from 6 to 7 at about 1.4×10^{13} W/cm^2, and yet K smoothly *decreases* through both of these thresholds. The fact that we find K to vary *smoothly* through a threshold may be correct for practical purposes but is not correct in principle; rather, the smooth variation is a consequence of using a (finite) discrete basis set which cannot, of course, reproduce the accumulation of resonances at (the right of) the threshold. In fact, the prominent resonance depicted in each of the curves in Fig. 7 to the right of the thresholds is presumably not the first, less prominent resonances lying closer to threshold being simply not detected with our finite basis.

We now turn our attention to harmonic generation. In Fig. 8 we show rates, both perturbative and nonperturbative,[29] versus the order of the harmonic at several different intensities for linearly polarized 1064-nm light incident on H(1s).[22,30] We see that perturbation theory yields a behavior with respect to order that is reasonable at low orders, but breaks down at high orders, more seriously for higher intensities I. The nonperturbative estimates of the rates for harmonic generation at first decrease sharply as the order increases, roughly level out into a plateau, and finally decrease beyond a certain order, $N_{\max}$ say. It is apparent that $N_{\max}$ increases with increasing I, and below we see that $N_{\max}$ also increases with increasing wavelength λ. It might be that, in analogy to radiative scattering[31] and multiphoton ionization,[32] $(N_{\max}-N_0)\hbar\omega$ is proportional to the ponderomotive shift P, but more extensive calculations are needed to establish

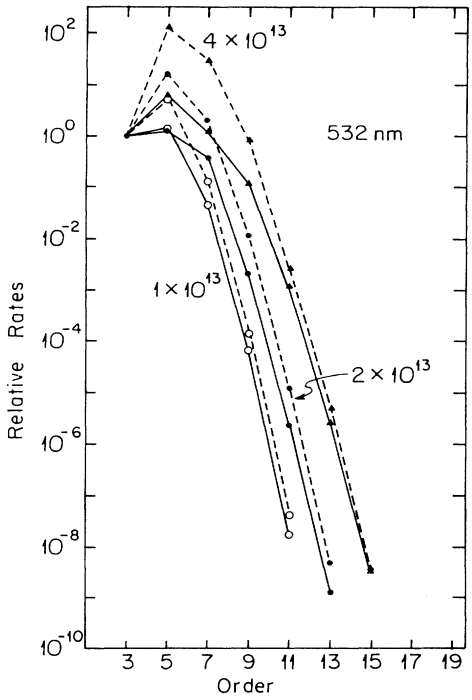

FIG. 9. Same as Fig. 8 but for an incident wavelength of 532 nm, and at the following intensities: —○—, 1×10^{13} W/cm^2; —●—, 2×10^{13} W/cm^2; —▲—, 4×10^{13} W/cm^2.

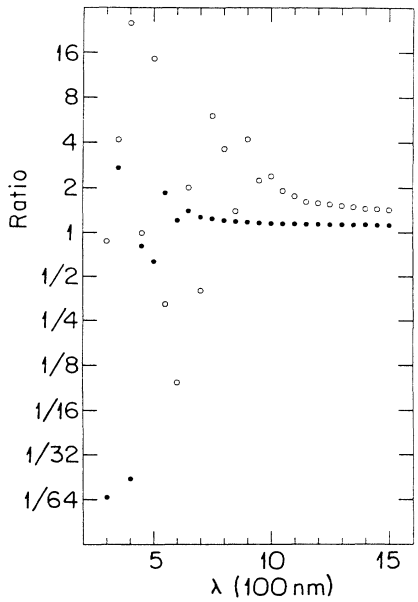

FIG. 10. Ratio of nonperturbative to perturbative rates for generation of the third- (●) and fifth- (○) order harmonics by linearly polarized light of intensity 1×10^{13} W/cm^2 incident on H(1s), for wavelengths increasing from 300 to 1500 nm by steps of 50 nm. Note that the scale of the vertical axis is logarithmic.

whether this is true. Of course, at high intensities saturation plays an important role. Note that the perturbative estimates of the rates do not exhibit a plateau; they peak roughly at N_0, the minimum number of photons required to ionize the atom. (This is true at all wavelengths.) Incidentally, the fact that, on the basis of our nonperturbative results, the strength of the ninth harmonic is larger than that of the seventh, shows that one cannot conclude that the breakdown of perturbation theory is signaled by an increase in the strength of the harmonics from one order to the next.

The appearance of an approximate plateau in the strength of the harmonics, at intermediate orders, was observed in a recent experiment.[12] However, it is difficult to make a direct comparison, not only because the rare gases rather than hydrogen were studied in this experiment, but also because we do not take into account the modification usually referred to as "phase matching." (Since harmonic generation leaves the atoms in the same initial state, it is impossible to know which atoms in the medium participated, and therefore the signal must be summed coherently over all atoms. This results in an enhancement factor when the phases of the incident and generated beams are appropriately matched.[33]) It is very difficult to evaluate the phase-matching effect correctly, particularly because the strength of each harmonic has a complicated dependence on I. If we were to assume that the phase-matching factor has the behavior[12] with respect

TABLE I. Ratios of nonperturbative to perturbative rates for Nth-order harmonic generation by linearly polarized light of intensity I (in W/cm^2) incident on H(1s). Columns labeled "Perturb." correspond to absolute differential perturbative rates, in a.u., for emission in the forward direction at 10^{13} W/cm^2. A number in brackets is the power of 10 by which the preceding number should be multiplied. Phase matching is not included.

	532 nm				1064 nm				
$N\backslash I$	1×10^{13}	2×10^{13}	4×10^{13}	Perturb.	1×10^{12}	5×10^{12}	1×10^{13}	2×10^{13}	Perturb.
3	1.8	3.6	2.9	1.6[−16]	1.0	1.1	1.1	1.3	3.7[−18]
5	6.1[−1]	2.4[−1]	2.0[−1]	1.2[−15]	1.1	1.3	1.9	3.2	9.2[−21]
7	6.4[−1]	6.5[−1]	9.9[−2]	3.0[−17]	1.2	3.6	1.0[1]	4.7	7.1[−22]
9	6.7[−1]	7.7[−1]	4.9[−1]	3.6[−20]	3.1	7.2[−1]	2.2[−1]	1.2[−1]	8.5[−20]
11	6.9[−1]	8.5[−1]	1.1	9.7[−24]	1.4	4.1[−3]	6.5[−3]	1.9[−4]	8.5[−18]
13	7.1[−1]	9.2[−1]	1.8	1.0[−27]	2.6	2.5[−2]	3.2[−3]	3.1[−5]	1.1[−17]
15	7.4[−1]	9.8[−1]	2.5	5.6[−32]	5.4	2.0[−1]	1.3[−2]	5.7[−5]	6.7[−19]
17	7.6[−1]	1.0	3.1	1.8[−36]	1.4[1]	1.1	2.1[−1]	1.5[−4]	7.4[−21]
19	7.7[−1]	1.0	3.6	3.8[−41]	3.9[1]	5.4	1.7	3.9[−3]	2.8[−23]

to order given in the weak-field approximation, our results would be modified significantly; for example, the perturbative rates would exhibit more of a plateau than a peak at intermediate orders. We will not pursue this further, but turn our attention to Fig. 9 where we show rates for harmonic generation by incident light of wavelength 532 nm, at various intensities (note that we have normalized the rates in Figs. 8 and 9 so that they have the same value for the third harmonic). At this wavelength the difference between the qualitative behaviors of the perturbative and nonperturbative results is not very striking, and there is no evidence of a plateau at intermediate orders. We did not find evidence of a plateau in the nonperturbative rates, at 1×10^{13} W/cm^2, for wavelengths smaller than 700 nm; a hint of a plateau is apparent at this wavelength, and this structure develops and extends to larger and larger order orders (e.g., up to the 21st order at 1200 nm) as the wavelength increases.

To appreciate the quantitative differences between the various rates we must normalize the nonperturbative results so that (in the present case where i is the $1s$ state and the incident light is linearly polarized) we have

$$\sum_n (\psi_{in}|\psi_{in})=1 ,$$

where

$$(a|b)=\int d^3x\, a(\mathbf{x})b(\mathbf{x}) .$$

(See Appendix A. The normalization of the perturbative rates is fixed by $|\psi_0\rangle=|\Phi_i\rangle$, the unperturbed initial-state vector.) Using this normalization, we present in Table I the ratios of the nonperturbative to the perturbative rates for Nth-order harmonic generation; absolute perturbative rates are also provided in Table I, so that the reader may obtain absolute nonperturbative rates from these ratios if needed. As above, these rates are for emission into the direction of incident propagation, and are summed over polarizations of emitted light. (In Ref. 10 we reported absolute perturbative rates which were, however, *integrated* over all angles of emission and summed over polarization and are therefore a factor of $8\pi/3$ larger than the rates for emission into the forward direction.) We see from Table I that at 1064 nm the nonperturbative rates, for a given order, do not have a simple power-law dependence on I. The nonperturbative and perturbative rates do not differ greatly at low orders (third or perhaps fifth order in Table I); for a given order, the agreement tends to improve (except when there are resonances) as the wavelength increases and/or as the intensity decreases. Roughly speaking, as the order increases the trend is for the perturbative rates to become at first too large, and subsequently too small. To illustrate these remarks more clearly, in Fig. 10 we show the (properly normalized) ratio of the nonperturbative to perturbative rates for third- and fifth-order harmonic generation versus wavelength λ, at an intensity 1×10^{13} W/cm^2. The reason that, for a given order N, perturbation theory tends to improve as the wavelength increases (in contrast to the case of ionization—recall Fig. 5) is simply that $N\hbar\omega$ becomes smaller than the difference between the ground and first excited energy levels of the atom as λ increases, and in this regime N ($\ll N_0$) photons do not greatly perturb the ground state (whereas $N\geq N_0$ photons ionize the atom). Similarly, the relative difference between perturbative and nonperturbative rates for Nth-order harmonic generation decreases as the ionic charge Z increases along the isoelectronic series of a species, at a fixed wavelength (these rates decrease rapidly with increasing Z).

ACKNOWLEDGMENTS

We thank Dr. A. L'Huillier for a helpful conversation on the subject of harmonic generation. This work was supported by the National Science Foundation under Grant No. PHY-8713196 and by the Faculty Research and Innovation Fund of the University of Southern California.

APPENDIX A: ORTHOGONALITY, NORMALIZATION, AND TIME REVERSAL

A. Overlap of Floquet state vectors

Let $|\Phi_j\rangle$ represent any unperturbed bound state j, and let E_j denote the (unperturbed) energy of the electron in that state. Let $|\psi_j(\tau)\rangle$ denote the Floquet eigenvector which approaches $|\Phi_j\rangle$ for vanishing intensity, $I\sim0$, and let ε_j be the corresponding eigenvalue. We introduce the *gauge-invariant* scalar product

$$X_{ji}(\zeta)=\frac{1}{2\pi}\int_0^{2\pi}d\tau\langle\psi_j(\tau)|e^{-\zeta r}|\psi_i(\tau)\rangle \tag{A1a}$$

$$=\sum_n\langle\psi_{jn}|^{-\zeta r}|\psi_{in}\rangle . \tag{A1b}$$

Recalling the boundary condition (1.7), we observe that if

$$\mathrm{Re}(\zeta)>-\mathrm{Im}(k_{jm'}+k_{im}) , \tag{A2}$$

for all integer m and m', the scalar products $\langle\psi_{jn}|e^{-\zeta r}|\psi_{in}\rangle$, which involve integrals over $\mathbf{x}$, exist. To define $X_{ji}(\zeta)$ over a wider range of ζ we analytically continue $X_{ji}(\zeta)$ from the region where inequality (A2) holds. As an example of analytic continuation, consider the integral

$$\int_0^\infty dr\, e^{ikr-\zeta r}dr=\frac{1}{\zeta-ik} . \tag{A3}$$

If $\mathrm{Re}(\zeta)>-\mathrm{Im}(k)$ the integrand decays exponentially for $r\sim\infty$, and the integral converges. For $\mathrm{Re}(\zeta)\leq-\mathrm{Im}(k)$ the integral does not formally exist, but the right-hand side of Eq. (A3) provides the analytic continuation into this region. The pole at $\zeta=ik$ arises because at this point the phase of the integrand is constant in r, and the integrand does not vanish for $r\sim\infty$. Hereafter, when we speak of $X_{ji}(\zeta)$ we mean the analytic continuation if (A2) does not hold. We assume that both Γ_i and Γ_j are small, in absolute magnitude, so that (A2) allows for small values of ζ. We are, of course, particularly interested in $X_{ji}(0)$. If $X_{ji}(\zeta)$ varies slowly in the neighborhood of $\zeta=0$ it is meaningful to speak of

$$X_{ji}(0)\exp[\varepsilon_j^*-\varepsilon_i)t/\hbar]$$

as the overlap of the state vectors which develop from states i and j.

Using Eqs. (1.3) and (A1a), assuming that the intensity I is constant, we have

$$\varepsilon_i X_{ji}(\zeta)=\frac{1}{2\pi}\int_0^{2\pi}d\tau\left\langle\psi_j(\tau)\left|e^{-\zeta r}\left[H_a+V(t)-i\hbar\frac{d}{dt}\right]\right|\psi_i(\tau)\right\rangle . \tag{A4}$$

We now integrate by parts over $\tau=\omega t$, noting that the surface term vanishes because of the periodicity of the τ integrand. Provided that inequality (A2) holds, H_a and $V(t)$ are both Hermitian in the scalar product on the right-hand side of Eq. (A4), and we obtain

$$\begin{aligned}\varepsilon_i X_{ji}(\zeta)&=\frac{1}{2\pi}\int_0^{2\pi}d\tau\left[\left\langle\psi_i(\tau)\right|\left[H_a+V(t)-i\hbar\frac{d}{dt}\right]e^{-\zeta^* r}\left|\psi_j(\tau)\right\rangle\right]^*\\&=\varepsilon_j^* X_{ji}(\zeta)+O(\zeta) ,\end{aligned} \tag{A5}$$

where in the second step we have assumed ζ to be small, and we have used Eq. (1.3) with i replaced by j. Now, $X_{ii}(\zeta)$ is sensitive to the value of ζ in the neighborhood of $\zeta=0$ because there is a nearby singularity. This singularity is analogous to the singularity at $\zeta=ik$ (with $k\approx 0$) in Eq. (A3), and it results from the cross terms involving

$$\exp[i(k_{im}-k_{im}^*)r]$$

in $\langle\psi_{in'}|\exp(-\zeta r)|\psi_{in}\rangle$; the phase of such cross terms is nearly constant in r if $\zeta\approx 0$. This problem does not arise for $X_{ji}(\zeta)$, $\varepsilon_i\neq\varepsilon_j$, barring the exceptional resonance when for each m there is an m' such that $k_{im}-k_{jm'}^*$ nearly vanishes. Assuming that the analytic continuation of the remainder $O(\zeta)$ vanishes at $\zeta=0$ if $\varepsilon_i\neq\varepsilon_j$, it follows that

$$(\varepsilon_i-\varepsilon_j^*)X_{ji}(0)=0,\quad \varepsilon_i\neq\varepsilon_j . \tag{A6}$$

Hence if $\varepsilon_i\neq\varepsilon_j$ we have that $X_{ji}(0)$ vanishes, that is, $|\psi_i(\tau)\rangle$ and $|\psi_j(\tau)\rangle$ are orthogonal. [Since $\exp(im\tau)|\psi_j(\tau)\rangle$ represents the same state as $|\psi_j(\tau)\rangle$, for m an integer, we have, more generally, that $\exp(im\tau)|\psi_j(\tau)\rangle$ and $\exp(il\tau)|\psi_l(\tau)\rangle$ are nearly orthogonal; the proof of this statement follows using the same reasoning as above.] We turn now to the question of the value of $X_{ii}(0)$ in the weak-field limit.

B. Discontinuity of $X_{ii}(0)$

We assume in this section that the intensity I is infinitesimally small. Thus the shift Δ_i and width Γ_i are also infinitesimal; consequently, inequality (A2) is satisfied for vanishingly small ζ.

The scattering-state eigenvectors, $|\Phi_{\mathbf{k}}^-\rangle$, of H_a, together with the bound-state eigenvectors, $|\Phi_\alpha\rangle$, form a complete set. (The superscript minus on $|\Phi_{\mathbf{k}}^-\rangle$ signifies outasymptote boundary conditions.) Using closure, with the normalization

$$\langle\Phi_{\mathbf{k}}^-|\Phi_{\mathbf{k}'}^-\rangle=\delta^3(\mathbf{k}-\mathbf{k}') , \tag{A7}$$

and putting $\zeta=0$ in Eq. (A1b), we can express $X_{ii}(0)$ as the sum of the bound-state contribution, S_b, and the scattering-state contribution, S_s:

$$S_b=\sum_n\sum_\alpha|\langle\Phi_\alpha|\psi_{in}\rangle|^2 , \tag{A8a}$$

$$S_s=\sum_n\int d^3k|\langle\Phi_{\mathbf{k}}^-|\psi_{in}\rangle|^2 . \tag{A8b}$$

Now $|\langle\Phi_\alpha|\psi_{in}\rangle|^2$ is of order I^n and therefore only the $n=0$ terms contribute to the sum on the right-hand side of Eq. (A8a). However, to zeroth order in I, we have $|\langle\Phi_\alpha|\psi_{i0}\rangle|^2=|\langle\Phi_\alpha|\Phi_i\rangle|^2=\delta_{\alpha i}$, and hence $S_b=1$. To determine S_s we first introduce the resolvent $G_a(E)=1/(E-H_a)$ and rewrite Eq. (1.6) as

$$|\psi_{in}\rangle=G_a(\varepsilon_i+n\hbar\omega)|f_{in}\rangle , \tag{A9a}$$

$$|f_{in}\rangle=V_+|\psi_{i,n-1}\rangle+V_-|\psi_{i,n+1}\rangle . \tag{A9b}$$

Defining $E_{in}=E_i+\Delta_i+n\hbar\omega$ and $E_k=(\hbar^2k^2/2\mu)$ we have

$$S_s=\sum_n\int d^3k\frac{|\langle\Phi_{\mathbf{k}}^-|f_{in}\rangle|^2}{(E_{in}-E_k)^2+(\Gamma_i/2)^2} . \tag{A10}$$

Using the following well-known representation of the Dirac δ function:

$$\pi\delta(x)=\eta/(x^2+\eta^2) , \tag{A11}$$

where η is positive but infinitesimal, Eq. (A10) becomes

$$\begin{aligned}S_s&=\frac{2\pi}{\Gamma_i}\sum_n\int d^3k|\langle\Phi_{\mathbf{k}}^-|f_{in}\rangle|^2\delta(E_k-E_{in})\\&=\frac{1}{\Gamma_i}\sum_{n\geq N_0}\Gamma_{in} ,\end{aligned} \tag{A12}$$

where

$$\Gamma_{in}=2\pi(\mu k_{in}/\hbar^2)\int d\hat{\mathbf{k}}|\langle\Phi_{\mathbf{k}_{in}}^-|f_{in}\rangle|^2 , \tag{A13}$$

and where $\mathbf{k}_{in}$ points along $\hat{\mathbf{k}}$, with $k_{in}=|\mathbf{k}_{in}|$, where k_{in} was defined by Eq. (1.8) above. Now, $\langle\Phi_{\mathbf{k}}^-|f_{in}\rangle$ with $\mathbf{k}=\mathbf{k}_{in}$ is, in the weak-field limit, the matrix element for n-photon ionization, with the electron ejected into the direction $\hat{\mathbf{k}}$. Since $(\mu k_{in}/\hbar^2)d\hat{\mathbf{k}}$ is the density of scattering states in a narrow energy interval centered at E_{in}, we have that $\Gamma_{in}/\hbar$ is the n-photon ionization rate integrated over all angles of electron emission. It follows from Eq. (A12) that $S_s=1$. In other words, if the field is infinitesimally weak the bound- and scattering-state contributions are each equal to 1, and we have $X_{ii}(0)=2$. Yet if the field were identically zero, $|\psi_{in}\rangle$ would vanish identically for $n\neq 0$ and we would have $S_s=0$, so that $X_{ii}(0)=1$. The reason for this peculiarity is that if the field is infinitesimally weak the electron remains bound

for all finite times, but after an infinite time the atom ionizes and the electron is in the continuum. In a time-independent theory the field persists for all time, and the contributions S_b and S_s are the contributions from finite and infinite times, respectively.

This result is, of course, sensitive to the order of the limits $I\to 0$ and $\zeta\to 0$. Were we to first let $I\to 0$ and then let $\zeta\to 0$ we would obtain $S_s=0$. The convergence factor $\exp(-\zeta r)$, with $\zeta\sim 0$, cuts off the region of asymptotically large r, which effectively cuts off the contribution from asymptotically large t since the distance traveled by a free electron is proportional to t.

C. Time reversal

Let the time-reversal operator T act on Eq. (1.1). Noting that T includes the operation of complex conjugation (it is *anti*unitary[34]) we obtain

$$\left[-i\hbar\frac{d}{dt}-H_a-V^*(t)\right]T|\Psi(t)\rangle=0\ . \tag{A14}$$

The atomic Hamiltonian is real, whereas in the velocity gauge $V(t)$ is not real because T anticommutes with $\mathbf{p}$. Since the field is treated as external, it is unaffected by T, which acts only on the atomic coordinates. However, if the field were included as part of the system the rotational sense of the polarization of the field would be reversed under time reversal. We therefore introduce

$$\bar{V}(t)=V_-e^{-i\omega t}+V_+e^{i\omega t}\ , \tag{A15}$$

which is the interaction of the electron with a field whose rotational sense of polarization is reversed (and whose phase may be shifted). Thus $\bar{V}(t)$ differs from $V(t)$ in that V_+ and V_- are interchanged. Now, there exists a constant $t_0=m_0\pi/\omega$, where m_0 is 0 or 1, such that

$$\bar{V}(t)=V^*(-t+t_0)\ . \tag{A16}$$

If $V(t)$ is real (as in the length gauge) we have $m_0=0$; if $V(t)$ is pure imaginary (as in the velocity gauge) we have $m_0=1$. Changing t to $-t+t_0$ in Eq. (A14), and using Eq. (A16), we obtain

$$\left[i\hbar\frac{d}{dt}-H_a-\bar{V}(t)\right]T|\Psi(-t+t_0)\rangle=0\ . \tag{A17}$$

In other words, if $|\Psi_i(t)\rangle$ satisfies Eq. (1.1), so does $T|\Psi_i(-t+t_0)\rangle$ if we replace $V(t)$ by $\bar{V}(t)$. Note that the Floquet eigenvalue spectrum cannot depend on the sense of the field polarization. Furthermore, if $|\bar{\Psi}_i(t)\rangle$ satisfies Eq. (1.1), when we replace $V(t)$ by $\bar{V}(t)$, then $T|\bar{\Psi}(-t+t_0)\rangle$ satisfies Eq. (1.1) in its original form, and if we make the Floquet ansatz

$$|\bar{\Psi}_i(t)\rangle\simeq e^{-i\varepsilon_i t/\hbar}|\bar{\psi}_i(\tau)\rangle\ ,$$

we have

$$T|\bar{\Psi}_i(-t+t_0)\rangle=e^{i\varepsilon_i^* t_0/\hbar}e^{-i\varepsilon_i^* t/\hbar}T|\bar{\psi}_i(-\tau+m_0\pi)\rangle\ . \tag{A18}$$

Hence if ε_i is an eigenvalue, so is ε_i^*. However, $T|\psi_i(-\tau+m_0\pi)\rangle$ satisfies an asymptotic boundary condition which differs from (1.7) in that the outgoing waves become *in*going waves.

It is very useful to define the *gauge-invariant* overlap

$$X_{ji}^T(\zeta)=\frac{1}{2\pi}\int_0^{2\pi}dt[\langle\bar{\psi}_j(-\tau+m_0\pi)|T^\dagger]e^{-\zeta r}|\psi_i(\tau)\rangle\ . \tag{A19}$$

(Note that m_0 is not invariant under a gauge transformation.) If we put $|\bar{\psi}_j(\tau)\rangle=\sum_n e^{-in\tau}|\bar{\psi}_{jn}\rangle$, we obtain

$$X_{ji}^T(\zeta)=\sum_n e^{-inm_0\pi}(\bar{\psi}_{jn}|e^{-\zeta r}|\psi_{in})\ , \tag{A20}$$

where by the scalar product $(a|b)$ we mean $(\langle a|T^\dagger)|b\rangle$, which is[34] equal to $[\langle b|(T|a\rangle)]^*$. If we ignore internal degrees of freedom, we have

$$(a|b)=\int d^3x\ a(\mathbf{x})b(\mathbf{x})\ ,$$

which differs from the usual scalar product $\langle a|b\rangle$ in that $a(\mathbf{x})$ is not complex conjugated. Noting that

$$\left[i\hbar\frac{d}{dt}+\varepsilon_j^*-H_a-V(t)\right]T|\bar{\psi}_j(-\tau+m_0\pi)\rangle=0\ , \tag{A21}$$

we can show, following the same analysis as in subsection A above, that

$$(\varepsilon_j-\varepsilon_i)X_{ji}^T=0\ . \tag{A22}$$

Hence if $\varepsilon_j\neq\varepsilon_i$ the vectors $|\bar{\psi}_i(\tau)\rangle$ and $T|\bar{\psi}_j(-\tau+m_0\pi)\rangle$ are orthogonal. Now, if $\bar{i}$ is the state reached by reversing the sign of the electronic angular momenta in state i, we have $T|\Phi_{\bar{i}}\rangle=|\Phi_i\rangle$ (ignoring a possible factor) and therefore in the weak-field limit $X_{\bar{i}\bar{i}}^T(0)=1$ (up to a phase factor). Furthermore, $X_{\bar{i}i}^T(\zeta)$ varies slowly with ζ in the neighborhood of $\zeta=0$, in contrast to $X_{ii}(\zeta)$. This suggests that an *a priori* knowledge of the value of $X_{\bar{i}i}^T(0)$, at intensities beyond the weak-field limit, might provide a convenient prescription for the normalization of $|\psi_i(\tau)\rangle$. This is a matter to which we now turn.

D. Normalization of $|\psi_i(\tau)\rangle$

There is a rather extensive literature on the question of the normalization of resonance wave functions in the context of *radiationless* atomic and nuclear *scattering*. For recent discussions, which contain many references to earlier work, see Watson[35] and Kukulin *et al.*[36] In our context, we have an electron which initially is truly bound. The exact state vector $|\Psi_i(t)\rangle$ has the normalization defined by

$$\langle\Psi_i(t)|\Psi_i(t)\rangle=\langle\Phi_i|\Phi_i\rangle\ . \tag{A23}$$

When we make the Floquet ansatz, we obtain

$$\langle\Psi_i(t)|\Psi_i(t)\rangle\simeq X_{ii}(0)e^{-\Gamma_i t/\hbar}\ . \tag{A24}$$

Whereas the exact value of $\langle\Psi_i(t)|\Psi_i(t)\rangle$ is constant in time, the Floquet ansatz yields a value which decays ex-

ponentially. The reason for this discrepancy is that when we make the Floquet ansatz, we treat the electron as having a definite (albeit complex) energy; in reality, the electron has a distribution of energies, with a width Γ_i, and the electron should be represented by a localized wave packet which is initially the bound-state vector $|\Phi_i\rangle$. The factor $\exp(-\Gamma_i t/\hbar)$ on the right-hand side of Eq. (A24) describes the electron loss from the bound state i, at the rate $\Gamma_i/\hbar$; the gain into the continuum, which should be $1-\exp(-\Gamma_i t/\hbar)$, is incorrectly treated by the Floquet ansatz because the Floquet state vector describes an electron which is at infinity, rather than localized. We can use the fact that the Floquet state vector describes (more or less) correctly the loss from state i to normalize $|\psi_i(\tau)\rangle$; see Eq. (3.5) of Ref. 15. However, this normalization is useful only if the field does not significantly distort the spatial probability distribution of the electron during the time that the field is turned on.

To explore whether $X^T_{\bar{i}i}(0)$ can be used to normalize $|\psi_i(\tau)\rangle$, we first continue to assume that I is constant in time. Equations (1.1) and (A17) imply

$$[\langle\bar{\Psi}_{\bar{i}}(-t+t_0)|T^\dagger]|\Psi_i(t)\rangle=\text{const}\ , \tag{A25}$$

where const is constant in time. Now, we have acted as if the field persists for all time. In fact, of course, the field is turned on at some finite time, $-\frac{1}{2}T_0$ say; we may take T_0 to be large and positive and (for the present purpose) treat I as constant for $t>-\frac{1}{2}T_0$. Equation (A16), and hence Eq. (A25), are valid only for $-\frac{1}{2}T_0<t<\frac{1}{2}T_0$. At time $t=\frac{1}{2}T_0\sim\infty$, $|\Psi_i(t)\rangle$ represents an electron which has escaped and is very far from its parent nucleus, while $T|\bar{\Psi}_{\bar{i}}(-t+t_0)\rangle$ describes an electron which is localized around the nucleus, with a spatial probability distribution $|\langle\mathbf{x}|\Phi_i\rangle|^2$. Hence the constant on the right-hand side of Eq. (A25) is of order $\exp(-\Gamma_i T_0/2\hbar)$. If we make the Floquet ansatz

$$|\Psi_j(t)\rangle\simeq\exp[-i\varepsilon_j(t+\tfrac{1}{2}T_0)/\hbar]|\psi_j(\tau)\rangle\ ,$$

where the factor $\exp(-i\varepsilon_j T_0/2\hbar)$ takes into account that the decay of state j begins at time $-T_0/2$, the right-hand side of Eq. (A25) becomes the *constant* quantity

$$\exp[-i\varepsilon_i(t_0+T_0)/\hbar]X^T_{\bar{i}i}(0)\ .$$

Equating this, up to a phase factor, with $\exp(-\Gamma_i T_0/2\hbar)$, and noting that $\Gamma_i t_0\ll 1$, it seems reasonable to normalize $|\psi_i(\tau)\rangle$ so that $X^T_{\bar{i}i}(0)=1$. Presumably this normalization remains appropriate even when the intensity varies in time, provided that the electron remains on the same eigenvalue curve, and is analagous to the normalization used[35,36] in time-independent radiationless scattering. However, a more rigorous justification of this normalization would be welcome.

APPENDIX B: DIPOLE MOMENT AND GAUGE INVARIANCE

A. Convergence of dipole moment $\mathbf{d}_N$

With reference to the boundary condition (1.7), and to Eq. (2.8b), the $\mathbf{x}$ integrand of $\mathbf{d}_{Nn}$ explodes exponentially and we must insert a factor $\exp(-\zeta r)$ into this integrand, thereby defining integrals $\mathbf{d}_{Nn}(\zeta)$ and $\mathbf{d}_N(\zeta)$. We may analytically continue these integrals (see Appendix A) to the point $\zeta=0$; it makes sense to identify $\mathbf{d}_N(0)$ with $\mathbf{d}_N$ provided that $\mathbf{d}_N(\zeta)$ varies slowly with ζ in the neighborhood of $\zeta=0$. However, each $\mathbf{d}_{Nn}(\zeta)$ has a singularity near to $\zeta=0$ because the phases of the cross terms in

$$f^*_{m,n-N}(\varepsilon_i,\hat{\mathbf{x}})f_{m,n}(\varepsilon_i,\hat{\mathbf{x}})e^{i(k_{im}-k^*_{im})r}/r^2$$

are nearly constant in r, and the contribution of these terms to the r integrand of $\mathbf{d}_{Nn}(\zeta)$ increases linearly with increasing r. Nevertheless, when we sum over n, the near divergent parts of the $\mathbf{d}_{Nn}(\zeta)$ cancel, and $\mathbf{d}_N(\zeta)$ has no nearby singularity at $\zeta=0$ so that it varies slowly in the neighborhood of $\zeta=0$. To see this, we recall that[16]

$$f_{mn}(\varepsilon_i,\hat{\mathbf{x}})=e^{i(n-m)\chi_m}J_{n-m}(\rho_m)f_m(\varepsilon_i,\hat{\mathbf{x}})\ , \tag{B1}$$

where $f_m(\varepsilon_i,\hat{\mathbf{x}})$ is the amplitude for the electron to absorb m real photons. There are infinitely many ways in which m real photons can be absorbed; $f_{mn}(\varepsilon_i,\hat{\mathbf{x}})$ is the amplitude for the electron to absorb n photons, m of which are real in the sense that the electron emerges asymptotically with a mean momentum equal to $\hbar k_{im}$. Thus $f_m(\varepsilon_i,\hat{\mathbf{x}})$ is a coherent sum over the $f_{mn}(\varepsilon_i,\hat{\mathbf{x}})$, with coefficients

$$\exp[i(m-n)\chi_m]J_{n-m}(\rho_m)\ ,$$

as follows from Eq. (B1) using the Graf addition formula for Bessel functions. Here, $J_n(z)$ is the regular Bessel function, and ρ_m and χ_m are both real quantities which depend on $\mathbf{k}_{im}=k_{im}\hat{\mathbf{x}}$ and on the vector potential $\mathbf{A}(t)$ of the field:

$$\mathbf{k}_{im}\cdot\boldsymbol{\alpha}(t)=\rho_m\sin(\omega t-\chi_m)\ , \tag{B2a}$$

$$\boldsymbol{\alpha}(t)=-(e/\mu c)\int^t dt'\,A(\mathbf{t}')\ . \tag{B2b}$$

Using the Graf addition formula, it follows from Eq. (2.9) that

$$\begin{aligned}\sum_n f^*_{m,n-N}(\varepsilon_i,\hat{\mathbf{x}})f_{m,n}(\varepsilon_i,\hat{\mathbf{x}})&=e^{iN\chi_m}|f_m(\varepsilon_i,\hat{\mathbf{x}})|^2\sum_n J_{n-N-m}(\rho_m)J_{n-m}(\rho_m)\\&=(-i)^N e^{iN\chi_m}J_N(0)|f_m(\varepsilon_i,\hat{\mathbf{x}})|^2\\&=\delta_{N0}|f_m(\varepsilon_i,\hat{\mathbf{x}})|^2\ .\end{aligned} \tag{B3}$$

Since $N\neq 0$, the singularities cancel.

B. Gauge transformation

We have used the velocity gauge to describe the laser field. In this gauge we have $V(t)=-(e/\mu c)\mathbf{A}(t)\cdot\mathbf{p}$; we have defined the scalar potential $\Phi(t)$ by

$$e\Phi(t)=-(e^2/2\mu c^2)A^2(t)\ , \tag{B4}$$

so that $V(t)$ contains no $A^2(t)$ term. Both $\mathbf{A}(t)$ and $\Phi(t)$ are assumed to be spatially homogeneous.

We may transform to a new gauge in which the vector

and scalar potentials are[19]

$$\mathbf{A}(t)\rightarrow \mathbf{A}'(\mathbf{x},t)=\mathbf{A}(t)+\nabla\Lambda(\mathbf{x},t)\ , \tag{B5a}$$

$$\Phi(t)\rightarrow\Phi'(\mathbf{x},t)=\Phi(t)-(1/c)\partial\Lambda(\mathbf{x},t)/\partial t\ , \tag{B5b}$$

where $\Lambda(\mathbf{x},t)$ does not depend on $\mathbf{p}$. The Hamiltonian $H(t)=H_a+V(t)$ transforms to $H'(t)=H_a+V'(t)$ where, introducing the unitary transformation operator

$$O(\mathbf{x},t)=e^{i(e/\hbar c)\Lambda(\mathbf{x},t)}\ , \tag{B6}$$

we have

$$O(\mathbf{x},t)\left[H(t)-i\hbar\frac{d}{dt}\right]O^{-1}(\mathbf{x},t)=H'(t)-i\hbar\frac{d}{dt}\ . \tag{B7}$$

A solution $|\Psi(t)\rangle$ of Eq. (1.1) transforms to[37]

$$|\Psi_i'(t)\rangle=O(\mathbf{x},t)|\Psi(t)\rangle\ . \tag{B8}$$

Provided that $V'(t)$ is periodic in t, with period $2\pi/\omega$, we may make the Floquet ansatz $|\Psi_i'(t)\rangle\simeq\exp(-i\varepsilon_i't/\hbar)|\psi_i'(\tau)\rangle$ in the new gauge, but the real part of the quasienergy need not be invariant under the gauge transformation since the zero of the energy scale is not physically significant (only energy differences are physically significant). On the other hand, the imaginary part of the quasienergy is proportional to the total ionization rate from state i, and this must be gauge invariant. It follows that

$$|\psi_i'(\tau)\rangle=e^{iPt/\hbar}O(\mathbf{x},t)|\psi_i(\tau)\rangle\ , \tag{B9}$$

where P is a constant, independent of i, equal to $\mathrm{Re}(\varepsilon_i'-\varepsilon_i)$. The operator $\exp(iPt/\hbar)O(\mathbf{x},t)$ is periodic in t, with period $2\pi/\omega$, and we can Fourier expand it:

$$O(\mathbf{x},t)=e^{-iPt/\hbar}\sum_n O_n(\mathbf{x})e^{-in\tau}\ . \tag{B10}$$

It follows that the harmonic components $|\psi_{in}'\rangle$ are related to the $|\psi_{in}\rangle$ by

$$|\psi_{im}'\rangle=\sum_n O_{m-n}(\mathbf{x})|\psi_{in}\rangle\ . \tag{B11}$$

This last result shows how the boundary condition (1.7) should be modified in the new gauge.

As an example, consider the length gauge, in which $V'(t)=-e\mathbf{x}\cdot\mathbf{E}(t)$ where $\mathbf{E}(t)$ is the (gauge-invariant) electric field vector. To pass to this gauge we choose

$$\Lambda(\mathbf{x},t)=-\mathbf{A}(t)\cdot\mathbf{x}+c\int^t dt'\Phi(t')\ , \tag{B12}$$

giving $\mathbf{A}'(\mathbf{x},t)=0$ and $\Phi'(t)=-\mathbf{E}\cdot\mathbf{x}$. Writing $\mathbf{A}(t)=\mathrm{Re}(\mathbf{A}_0e^{-i\tau})$ we have

$$(e/\hbar c)c\int^t dt'\Phi(t')=-Pt/\hbar+h(\tau)\ , \tag{B13}$$

where $P=e^2A_0^2/(4\mu c^2)$ is the ponderomotive energy shift, and where $h(\tau)$ is a periodic function of τ with period 2π. [In the velocity gauge, with the A^2 term removed from $V(t)$, the continuum threshold does not shift, whereas in the length gauge the threshold shifts by P.] Consequently, we have

$$O_n(\mathbf{x})=\frac{1}{2\pi}\int_0^{2\pi}e^{in\tau}e^{-i(e/\hbar c)\mathbf{A}(t)\cdot\mathbf{x}+ih(\tau)}\ . \tag{B14}$$

Here $O_n(\mathbf{x})$ is a generalized Bessel function.[38] If the polarization is circular we have $h(\tau)=0$ and the generalized Bessel function simplifies to the standard one:

$$O_n(\mathbf{x})=e^{in(\theta-\pi/2)}J_n(ar)\ , \tag{B15}$$

where $a=(e/\hbar c)|\mathbf{A}_0|/\sqrt{2}$, and where θ is the angle $\pm\tan^{-1}(y/x)$, with the sign determined by whether the light is right or left circularly polarized. Combining Eqs. (1.7), (B1), (B11), and (B15) we find, after using the Graf addition formula and the asymptotic form of the Bessel function for large argument,

$$\langle\mathbf{x}|\psi_{in}'\rangle\sim(2/\pi ar)^{1/2}\sum_m e^{i(n-m)(\theta-\pi/2)}\cos[ar-\rho_m\sin(\chi_m-\theta)+(n-m)\pi/2-\pi/4]f_m(\varepsilon_i,\hat{\mathbf{x}})r^{i\nu_m}\exp(ik_mr)/r,\quad r\sim\infty \tag{B16}$$

for circular polarization, where we have ignored mathematical questions of uniform convergence, etc. This boundary condition, which does not apply in the weak-field limit where $a\sim0$ (since we have assumed that $ar\sim\infty$), differs significantly from (1.7). By using the properties[38] of the generalized Bessel functions, Eq. (B16) can be generalized to arbitrary polarization.

C. Gauge invariance

The $\mathbf{d}_{Nn}(\xi)$ are not separately gauge invariant but, as we now show, the sum $\mathbf{d}_N(\xi)$ is gauge invariant for ξ small. We first introduce the interaction $V_{\mathrm{sp}}(t)=V_{\mathrm{sp}}e^{i\Omega t}$ which gives rise to the spontaneous emission of a photon of frequency $\Omega=N\omega$ and polarization $\hat{\boldsymbol{\varepsilon}}$. If we represent the vacuum field in the length gauge, we have $V_{\mathrm{sp}}=\beta e\hat{\boldsymbol{\varepsilon}}^*\cdot\mathbf{x}$, where β is a constant (which depends on Ω). We can use Eqs. (2.8) and (1.4) to write

$$\hat{\boldsymbol{\varepsilon}}^*\cdot\mathbf{d}_N(\xi)=\frac{1}{2\pi\beta}\int_0^{2\pi}d\tau\langle\psi_i(\tau)|e^{-\xi r}V_{\mathrm{sp}}(t)|\psi_i(\tau)\rangle\ . \tag{B17}$$

Let us now include $V_{\mathrm{sp}}(t)$ in the Hamiltonian $H(t)$; thus $H(t)=H_a+V(t)+V_{\mathrm{sp}}(t)$. Using Eq. (1.3) [we determine $|\psi_i(\tau)\rangle$ without including $V_{\mathrm{sp}}(t)$] we may write

$$\hat{\varepsilon}^*\cdot\mathbf{d}_N(\zeta)=\frac{1}{2\pi\beta}\int_0^{2\pi}d\tau\left\langle\psi_i(\tau)\left|e^{-\zeta r}\left[H(t)-\varepsilon_i-i\hbar\frac{d}{dt}\right]\right|\psi_i(\tau)\right\rangle . \tag{B18}$$

We now make a gauge transformation. We attach subscripts l and sp to the transformation operators appropriate to the laser and vacuum fields, respectively; thus $O(\mathbf{x},t)=O_l(\mathbf{x},t)O_{\rm sp}(\mathbf{x},t)$. Since we retain $V_{\rm sp}(t)$ only through first order (spontaneous emission is a weak process) we may insert $O_{\rm sp}(\mathbf{x},t)$ to the left (or to the right) of $V_{\rm sp}(t)$ in Eq. (B17); this introduces an error of second order. We may therefore insert $O_{\rm sp}(\mathbf{x},t)$ to the left (but *not* to the right) of $[H(t)-\varepsilon_i-i\hbar(d/dt)]$ in Eq. (B18). We do this, and we also insert $1=O_{\rm sp}^{-1}(\mathbf{x},t)O_{\rm sp}(\mathbf{x},t)$ to the right of $[H(t)-\varepsilon_i-i\hbar(d/dt)]$. Expressing the bra and ket Floquet state vectors in terms of their transforms, according to Eq. (B9) but with $O=O_l$, and recalling that $O_l^{-1}(\mathbf{x},t)=O_l(\mathbf{x},t)^\dagger$, we obtain, after noting that $O_l(\mathbf{x},t)$ and $O_{\rm sp}(\mathbf{x},t)$ commute with each other and with $\exp(-\zeta r)$, and using Eq. (B7),

$$\hat{\varepsilon}^*\cdot\mathbf{d}_N(\zeta)=\frac{1}{2\pi\beta}\int_0^{2\pi}d\tau\left\langle\psi_i'(\tau)\left|e^{-\zeta r}\left[H'(\tau)+\varepsilon_i'-i\hbar\frac{d}{dt}\right]O_{\rm sp}(\mathbf{x},t)\right|\psi_i'(\tau)\right\rangle . \tag{B19}$$

We now integrate by parts over $\tau=\omega t$, use the Hermiticity of $H'(t)$, and use (the primed form of) Eq. (1.3) to yield

$$\hat{\varepsilon}^*\cdot\mathbf{d}_N(\zeta)=\frac{1}{2\pi\beta}\int_0^{2\pi}d\tau\langle\psi_i'(\tau)|V_{\rm sp}'(t)e^{-\zeta r}O_{\rm sp}(\mathbf{x},t)|\psi_i'(\tau)\rangle+O(\zeta) . \tag{B20}$$

We may neglect $O_{\rm sp}(\mathbf{x},t)$ in the integrand on the right-hand side of Eq. (B20), thereby introducing an error of second order; comparing with Eq. (B17) we see that $\hat{\varepsilon}^*\cdot\mathbf{d}_N(0)$ is gauge invariant, assuming that the analytic continuation of the remainder $O(\zeta)$ vanishes at $\zeta=0$.

Note that the expressions derived in the Appendix of Ref. 16 for the N-photon ionization amplitude are not gauge invariant; these expressions were derived in the velocity gauge. While the velocity gauge is computationally the most convenient, an exact calculation should of course be gauge invariant.

APPENDIX C: BEHAVIOR OF FLOQUET EIGENVALUES AND EIGENVECTORS AT AN INTERMEDIATE RESONANCE

In this appendix we consider the case of an intermediate resonance between the states i and j; we suppose that the eigenvalues ε_j, $i\neq j$, differ by very nearly an integral multiple m of $\hbar\omega$. We summarize, with several helpful modifications, some useful results obtained earlier by Gontier and Trahin,[20] and by Holt *et al.*,[21] under the assumption that the field is sufficiently weak that, at resonance, the atom can be viewed as consisting of just two bound levels, i and j. Within this two-level model, the electron state vector can be expressed as

$$|\Psi(t)\rangle\simeq\sum_{\alpha=i,j}a_\alpha(t)e^{-i(E_\alpha+\delta_\alpha-i\gamma_\alpha/2)t/\hbar}|\Phi_\alpha\rangle , \tag{C1}$$

where we have allowed for the shift and decay (into the continuum) of level α through the inclusion of δ_α and γ_α. (Here δ_α and γ_α are the shifts and widths that would be obtained if the coupling between states i and j were turned off.) If we make the rotating-wave approximation, the coefficients $a_\alpha(t)$ are coupled through the equations (where the dot means time derivative)

$$i\dot{a}_i=(\Omega_0/2)e^{i\phi}a_j e^{i\delta\omega_c t} , \tag{C2a}$$

$$i\dot{a}_j=(\Omega_0/2)e^{-i\phi}a_i e^{-i\delta\omega_c t} , \tag{C2b}$$

where $\hbar\Omega_0$ is the coupling energy, with ϕ a coupling phase, and where $\delta\omega_c$ is the complex detuning, which is given in terms of the real detuning

$$\delta\omega=m\omega-(E_j+\delta_j-E_i-\delta_i)/\hbar \tag{C3a}$$

by

$$\delta\omega_c=\delta\omega+i(\gamma_j-\gamma_i)/2\hbar . \tag{C3b}$$

Solving Eqs. (C2) with I fixed, we obtain the two Floquet eigenvectors

$$|\Psi_\pm(t)\rangle=|\psi_\pm(\tau)\rangle e^{-i\varepsilon_\pm t/\hbar} , \tag{C4a}$$

$$|\psi_\pm(\tau)\rangle=N_\pm(e^{\pm\xi/2}|\Phi_i\rangle\pm e^{\mp\xi/2}e^{i\phi}e^{-im\tau}|\Phi_j\rangle) , \tag{C4b}$$

where $N_\pm$ are normalization constants, where

$$\sinh(\xi)=\delta\omega_c/\Omega_0 , \tag{C5}$$

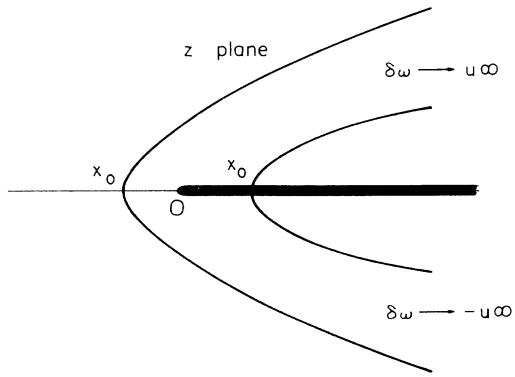

FIG. 11. Two possible (parabolic) trajectories of $z=(\delta\omega_c)^2+\Omega_0^2$ as $\delta\omega$ varies from $u\infty$ to $-u\infty$, where u is the sign of $\gamma_j-\gamma_i$. The intensity is held fixed. A trajectory crosses the real axis at x_0, where x_0 depends on the intensity and is positive or negative according to whether $2\hbar\Omega_0$ is greater than or less than $|\gamma_j-\gamma_i|$.

and where the Floquet eigenvalues are

$$\varepsilon_{\pm}=\frac{1}{2}\left[E_i+\delta_i+E_j+\delta_j-\frac{i}{2}(\gamma_i+\gamma_j)-m\hbar\omega\pm\hbar\Omega_c\right], \tag{C6}$$

with Ω_c the complex generalized Rabi frequency:

$$\Omega_c=[(\delta\omega_c)^2+\Omega_0^2]^{1/2}. \tag{C7}$$

Now Ω_c, as a function of $z=(\delta\omega_c)^2+\Omega_0^2$, has two square root branches, and we must be careful to specify which branch Ω_c is on. We define the principal branch as the one which is real and positive when z lies just above the positive real axis in the complex z plane. We draw a branch cut along this axis, and the secondary branch is reached by crossing this branch cut. On the principal branch we have $0\le\arg(\Omega_c)<\pi$ while on the secondary branch we have $-\pi\le\arg(\Omega_c)<0$. We choose Ω_c so that it is on the principal branch if $\mathrm{Im}(z)\ge 0$. In Fig. 11 we show two possible trajectories of z as $\delta\omega$ varies from $-\infty$ to ∞ with the intensity fixed. When $\delta\omega$ passes through zero, a trajectory crosses the real axis, at $x_0=\Omega_0^2-(\gamma_j-\gamma_i)^2/4\hbar^2$. If x_0 is positive, the trajectory crosses the branch cut and Ω_c changes branches. If $x_0=0$ the trajectory passes through the branch point singularity at the origin, and Ω_c is subsequently undefined. (This, of course, indicates that the dynamics of the passage through resonance is rather complicated when $|\gamma_j-\gamma_i|\sim 2\hbar\Omega_0$.) If x_0 is negative, Ω_c remains on the same branch. As long as the branch of Ω_c can be specified unambiguously, we may solve Eq. (C5) as

$$\xi=\ln[(\delta\omega_c+\Omega_c)/\Omega_0]. \tag{C5'}$$

It follows that as $|\delta\omega|\to\infty$ we have $\Omega_c\to s\delta\omega$ and $\xi\to s\infty$ where s is the sign of either $\delta\omega$ or $\gamma_j-\gamma_i$, according to whether x_0 is positive or negative, respectively. With this definition of s we have in either the far-off-resonance limit $|\delta\omega|\sim\infty$, or the vanishing intensity limit $I\sim 0$, that

$$|\Psi_s(t)\rangle\simeq e^{-i(E_i+\delta_i-i\gamma_i/2)t/\hbar}|\Phi_i\rangle, \tag{C8a}$$

$$|\Psi_{-s}(t)\rangle\simeq e^{-i(E_j+\delta_j-i\gamma_j/2)t/\hbar}|\Phi_j\rangle. \tag{C8b}$$

Exactly at resonance, where $\delta\omega=0$, we have the following.

(i) *If* $|\gamma_j-\gamma_i|\ll 2\hbar\Omega_0$:

$$|\Psi_{\pm}(t)\rangle\simeq\frac{1}{\sqrt{2}}(e^{-i(E_i+\delta_i)t/\hbar}|\Phi_i\rangle \pm e^{-i(E_j+\delta_j)t/\hbar}e^{i\phi}|\Phi_j\rangle). \tag{C9}$$

(ii) *If* $|\gamma_j-\gamma_i|\gg 2\hbar\Omega_0$:

$$|\Psi_u(t)\rangle\simeq e^{-i\varepsilon_u t/\hbar}|\Phi_i\rangle, \tag{C10a}$$

$$|\Psi_{-u}(t)\rangle\simeq e^{-i\varepsilon_{-u}t/\hbar}|\Phi_j\rangle, \tag{C10b}$$

where u denotes the sign of $\gamma_j-\gamma_i$.

Near resonance the Floquet eigenvalues are the following.

(i) *If* $|\gamma_j-\gamma_i|\ll 2\hbar\Omega_0$:

$$\mathrm{Re}(\varepsilon_{\pm})\simeq\tfrac{1}{2}(E_i+\delta_i+E_j+\delta_j\pm\hbar\Omega), \tag{C11a}$$

$$\Omega=[(\delta\omega)^2+\Omega_0^2]^{1/2}, \tag{C11b}$$

$$\mathrm{Im}(\varepsilon_{\pm})\simeq\tfrac{1}{4}[-(\gamma_i+\gamma_j)\pm(\delta\omega/\Omega)(\gamma_j-\gamma_i)]. \tag{C11c}$$

(ii) *If* $|\gamma_j-\gamma_i|\gg 2\hbar\Omega_0$:

$$\mathrm{Re}(\varepsilon_{\pm})\simeq\tfrac{1}{2}(E_i+\delta_i+E_j+\delta_j-\hbar\omega\pm u\hbar\delta\omega), \tag{C12a}$$

$$\mathrm{Im}(\varepsilon_u)\simeq-\tfrac{1}{2}[\gamma_i+u\gamma_{\mathrm{ex}}(\delta\omega)], \tag{C12b}$$

$$\mathrm{Im}(\varepsilon_{-u})\simeq-\tfrac{1}{2}[\gamma_j-u\gamma_{\mathrm{ex}}(\delta\omega)], \tag{C12c}$$

$$\gamma_{\mathrm{ex}}(\delta\omega)=2(\Omega_0/2)^2\frac{|\gamma_j-\gamma_i|/2}{[(\delta\omega)^2+(\gamma_j-\gamma_i)^2/4\hbar^2]}. \tag{C12d}$$

In case (i) the real parts of the eigenvalues $\varepsilon_{\pm}$ exhibit an avoided crossing at resonance, with a gap of magnitude $\hbar\Omega_0$. On the other hand, the imaginary parts of $\varepsilon_{\pm}$ exhibit a true crossing at resonance. The complex Rabi frequency Ω_c switches branches as the resonance is passed. The Floquet eigenvectors are equal mixtures of the atomic bound-state vectors at resonance. In contrast, in case (ii) the real parts of the eigenvalues exhibit a true crossing at resonance, the imaginary parts of $\varepsilon_{\pm}$ exhibit an avoided crossing with a gap of magnitude $|\gamma_j-\gamma_i|/2-\gamma_{\mathrm{ex}}(0)$, and Ω_c remains on the same branch as the resonance is passed. Note that in order to fulfill the criterion of case (ii) we must have $\gamma_{\mathrm{ex}}(\delta\omega)\ll|\gamma_j-\gamma_i|$ and either $\gamma_j\gg\gamma_i$ or $\gamma_i\gg\gamma_j$. We may identify $\gamma_{\mathrm{ex}}(\delta\omega)$ with the excitation rate of state j from state i. This follows from Fermi's golden rule, noting that the quantity in square brackets on the right-hand side of Eq. (C12d) provides a representation of the Dirac δ function; cf. Eq. (A11) with $x=\delta\omega$ and $\eta=|\gamma_j-\gamma_i|/2$. (Energy conservation need be satisfied only to within the width $|\gamma_j-\gamma_i|$.) The interpretation of Eqs. (C12b) and (C12c) is now straightforward. Thus, if u [the sign of $(\gamma_j-\gamma_i)$] is positive, $-2\,\mathrm{Im}(\varepsilon_u)$ is the rate of decay γ_i of state i into the continuum plus the rate of excitation from i to j; once the electron reaches the state j, the atom ionizes at the rate γ_j. On the other hand, $-2\,\mathrm{Im}(\varepsilon_{-u})$ is the rate of decay γ_j of state j into the continuum, minus the rate of deexcitation $\gamma_{\mathrm{ex}}(\delta\omega)$ of state j to i. The roles of i and j are reversed if u is negative. Note that at resonance the Floquet eigenvectors are single atomic bound-state vectors.

We may write $|\psi_i(\tau)\rangle$ and $|\psi_j(\tau)\rangle$ in place of $|\psi_{\pm}(\tau)\rangle$, where the signs $\pm$ are correlated with i and j according to Eqs. (C8). In general, ξ is complex and $|\psi_i(\tau)\rangle$ and $|\psi_j(\tau)\rangle$ are not orthogonal with respect to the overlap $X_{ji}(0)$ defined by Eqs. (A1). However, $|\psi_i(\tau)\rangle$ and $|\psi_j^{\sim}(\tau)\rangle$ are orthogonal with respect to the overlap $X_{ji}^{T}(0)$ defined by Eqs. (A19) and (A20). This may easily be verified after noting that when we reverse the sense of the field polarization and the sign of the electronic angular momenta, we must complex conjugate the coupling matrix element $(\Omega_0/2)e^{i\phi}$, so that $\phi\to-\phi$.

[1]S.-I Chu and J. Cooper, Phys. Rev. A **32**, 2769 (1985).
[2]R. Shakeshaft and X. Tang, Phys. Rev. A **36**, 3193 (1987).
[3]R. M. Potvliege and R. Shakeshaft, Phys. Rev. A **38**, 1098 (1988).
[4]A. Giusti-Suzor and P. Zoller, Phys. Rev. A **36**, 5178 (1987).
[5]M. Crance, J. Phys. B **21**, 2697 (1988).
[6]We note, however, that rates for harmonic generation for xenon have been calculated by K. C. Kulander and B. W. Shore, Phys. Rev. Lett. **62**, 524 (1989), by numerically solving the time-dependent Schrödinger equation in the Hartree-Fock approximation.
[7]Y. Gontier and M. Trahin, IEEE J. Quantum Electron. **QE-18**, 1137 (1982).
[8]Bo Gao and A. F. Starace, Phys. Rev. A **39**, 4550 (1989).
[9]L. Pan, K. T. Taylor, and C. W. Clark, Phys. Rev. A **39**, 4894 (1989).
[10]R. M. Potvliege and R. Shakeshaft, Z. Phys. D **11**, 93 (1989).
[11]A. Mc Pherson, G. Gibson, H. Jara, U. Johann, T. S. Luk, I. McIntyre, K. Boyer, and C. K. Rhodes, J. Opt. Soc. Am. B **4**, 595 (1987).
[12]M. Ferray, A. L'Huillier, X. F. Li, L. A. Lompré, G. Mainfray, and C. Manus, J. Phys. B **21**, L31 (1988); X. F. Li, A. L'Huillier, M. Ferray, L. A. Lompré, and G. Mainfray, Phys. Rev. A **39**, 5751 (1989).
[13]See, in particular, A. Maquet, S.-I Chu, and W. P. Reinhardt, Phys. Rev. A **27**, 2946 (1983).
[14]For a review of Floquet methods see S.-I Chu, Adv. At. Mol. Phys. **21**, 197 (1985), and N. L. Manakov, V. D. Ovsiannikov, and L. P. Rapport, Phys. Rep. **141**, 319 (1986). For a review of the use of complex scaling in resonance phenomena see B. R. Junker, Adv. At. Mol. Phys. **18**, 207 (1982) (see, in particular, Sec. II of this paper in relation to the discussions of the properties of Floquet eigenstates of Appendix A).
[15]R. M. Potvliege and R. Shakeshaft, Phys. Rev. A **38**, 4597 (1988). We take this opportunity to correct two misprints. On p. 4601, 3 lines from bottom, right-hand column, replace $\Gamma_i=-i\eta$ by $\Gamma_i=-\eta$. On p. 4602, line 1, left-hand column, replace $\Delta_i+\eta$ by $\Delta_i+i\eta$. Also, note that λ_i, defined by Eq. (3.16), is of order Γ_i.
[16]R. M. Potvliege and R. Shakeshaft, Phys. Rev. A **38**, 6190 (1988).
[17]See, e.g., J. H. Shirley, Phys. Rev. **138**, B979 (1965).
[18]R. M. Potvliege and R. Shakeshaft, Phys. Rev. A **39**, 1545 (1989).
[19]J. D. Jackson, *Classical Electrodynamics*, 2nd ed. (Wiley, New York, 1975).
[20]Y. Gontier and M. Trahin, Phys. Rev. A **19**, 264 (1979).
[21]C. R. Holt, M. G. Raymer, and W. P. Reinhardt, Phys. Rev. A **27**, 2971 (1983).
[22]All the numerical results presented in this work are converged with respect to the number of harmonic components, angular momenta, basis functions, etc., included in the calculations, the only exception being that convergence of the results shown in Fig. 3 is not always achieved with respect to the number of angular momenta (however, that does not affect these results *qualitatively*). In the case of Fig. 3, the basis set consisted of 19 harmonic components $|\psi_{jm}\rangle$ with the photon index m in the range $-3\le m\le 15$. Each harmonic component was expanded on a basis of 40 complex Sturmian functions for each orbital angular momentum quantum number l, with l in the range $0\le l\le 7$. The wave number κ of the Sturmian functions was chosen so that $|\kappa|=0.14$ or 0.63, and $\arg(\kappa)=70°$. In the case of the results shown in Fig. 4, the basis set consisted of 33 harmonic components $|\psi_{jm}\rangle$ with $-8\le m\le 24$; each harmonic component was expanded on 35 complex Sturmian functions for each value of l ($0\le l\le 13$) with $|\kappa|=0.2$ or 0.63 and $\arg(\kappa)=70°$ (smaller basis sets were used at low intensity.) In the case of the results shown in Fig. 8 for 2×10^{13} W/cm^2, the basis set consisted of 49 harmonic components with $-24\le m\le 24$, each of them expanded on 50 complex Sturmian functions for each value of l ($0\le l\le 12$) with $|\kappa|=0.44$ and $\arg(\kappa)=70°$ (smaller basis sets were satisfactory at lower intensities).
[23]We note that associated with each dominant resonance pole are infinitely many "shadow" poles which lie further from the physical energy axis than the dominant pole (see Ref. 16). When a dominant pole which corresponds to a bound state at $I=0$ crosses an N-photon ionization threshold with $N>0$, a shadow pole interchanges roles with the dominant pole, that is, a shadow pole becomes the dominant pole. This occurs, for example, when ε_{15} crosses the 12-photon ionization threshold in Fig. 3. Only dominant poles are shown in Fig. 3. Examples of shadow poles becoming dominant poles as the intensity increases have been clearly identified in the case of an electron undergoing photodetachment in a model one-dimensional short-range potential; see M. Dörr and R. M. Potvliege (unpublished).
[24]Note that Ω_0 and γ_{15} vanish as $I^{N_j/2}$ and I^{N_0}, respectively, for $I\sim 0$, so that γ_{15} is much smaller than $\hbar\Omega_0$ unless the principal quantum number of j is very large.
[25]As shown by Cerjan and Kosloff [J. Phys. B **20**, 4441 (1987)] and by Javanainen and Eberly [J. Phys. B **21**, L93 (1988)] for one-dimensional cases, the Reiss theory [L. V. Keldysh, Zh. Eksp. Teor. Fiz. **47**, 1945 (1964) [Sov. Phys.—JETP **20**, 1307 (1965)]; F. H. M. Faisal, J. Phys. B **6**, L89 (1973); H. R. Reiss, Phys. Rev. A **22**, 1786 (1980)] may grossly underestimate photodetachment rates. At 1064 nm for intensities between 0.5×10^{13} and 3.0×10^{13} W/cm^2, the total ionization rates predicted by this simple theory are about three orders of magnitude smaller than the nonperturbative rates presented in Fig. 4.
[26]R. R. Freeman, P. H. Bucksbaum, H. Milchberg, S. Darack, D. Shumacher, and M. E. Geusic, Phys. Rev. Lett. **59**, 1092 (1987).
[27]W. E. Cooke, R. R. Freeman, and T. J. McIlrath, in Proceedings of the 4th Topical Conference on Laser Techniques in the XUV, Cape Cod, 1988 (unpublished).
[28]Recently Wolff *et al.* published experimental data on the ionization of H(1*s*) at wavelengths of 532 and 1064 nm, and intensities up to some 10^{13} W/cm^2. They measure an index of nonlinearity which at low intensities is 6 at 532 nm and 12 at 1064 nm, and which decreases as I increases, but presumably because of saturation. Unfortunately, as Wolff *et al.* point out, it is difficult to compare in detail experimental and theoretical data on the index of nonlinearity, for several reasons [B. Wolff, H. Rottke, D. Feldmann, and K. H. Welge, Z. Phys. D **10**, 35 (1988)].
[29]The (nonperturbative) dipole moment $\mathbf{d}_N$, of Eq. (2.8a), does not converge when it is expanded on our complex Sturmian basis and we use Padé summation to obtain a finite result. The nonconvergence is due to the fact that $\langle\mathbf{x}|\psi_{in}\rangle$ contains outgoing waves, while $\langle\psi_{i,n-N}|\mathbf{x}\rangle$ contains ingoing waves, and a Sturmian basis with only a single wave number cannot span the space of both outgoing and ingoing waves. See Refs. 3 and 18 and also R. M. Potvliege and R. Shakeshaft, J. Phys. B **21**, L645 (1988) for further discussion. The perturbative estimate of $\mathbf{d}_N$ does converge because in lowest-order perturba-

tion theory, $\langle \psi_{i,n-N} | \mathbf{x} \rangle$ contains *damped* ingoing waves for $0 \leq n \leq N$.

[30]Effects arising from the finite mass of the nucleus can affect in a significant way rates for high-order multiphoton processes, as noted in Refs. 10 and 18. All the numerical results presented here, for photoionization or harmonic generation, are for hydrogen. The perturbative results shown in Fig. 8 differ by up to 42% (for the 19th harmonic) from the corresponding results for deuterium; however, the nonperturbative rates for these two isotopes do not differ by more than 10%.

[31]R. Shakeshaft, Phys. Rev. A **28**, 667 (1983).

[32]F. J. Berson, J. Phys. Rev. B **8**, 3078 (1975). See also pp. 717–718 of R. Shakeshaft, J. Opt. Soc. Am. B **4**, 705 (1987).

[33]See, e.g., R. Loudon, *The Quantum Theory of Light*, 2nd ed. (Oxford, New York, 1983); J. F. Reintjes, *Nonlinear Optical Parametric Processes in Liquid and Gases* (Academic, Orlando, 1984).

[34]A. Messiah, *Quantum Mechanics* (Wiley, New York, 1962), Chap. XV.

[35]D. K. Watson, Phys. Rev. A **34**, 1016 (1986).

[36]V. I. Kukulin, V. M. Krasnopol'sky, and J. Horáček, *Theory of Resonances* (Academia, Prague, 1989).

[37]C. Cohen-Tannoudji, B. Diu, and F. Laloe, *Quantum Mechanics* (Hermann-Wiley, Paris, 1977), Vol. 1.

[38]E. J. Kelsey and L. Rosenberg, Phys. Rev. A **19**, 756 (1979).